

University of Ottawa

Geometrical modeling of the heart

by

Olivier Rousseau

Department of Mathematics and Statistics
Faculty of Graduate Studies

Specialized Comprehensive Examination
presented to the Faculty of Graduate Studies

february 2007

© Olivier Rousseau, 2006

University of Ottawa

Faculty of Graduate Studies

This Comprehensive Exam named

Geometrical modeling of the heart

presented by

Olivier Rousseau

is evaluated by the following persons :

Yves Bourgault

(supervisor)

Paul-Eugène Parent

(co-supervisor)

Arian Novruzi

(jury member)

David Admunsen

(jury member)

ABSTRACT

This report has been written as part of Olivier Rousseau PhD project. It is presented as a Comprehensive Examination.

The main goal of this PhD project is to construct a precise 3D geometrical model of the human heart. Geometrical characteristics are to be extracted from high resolution medical images such as CT or MRI scans. The main challenge is to denoise and segment these images. The segmentation process consists in extracting the contours of the heart from the images. PDE methods will be preferred.

This report is a survey of the main PDE techniques in image processing. It focuss on the denoising problem and the segmentation problem. First, the type of data to process is presented in Chapter 1. The large size of the data sets restricts the type of methods of resolution to be used. Chapter 2 presents some background of Measure Theory and Calculus of Variations. These notions will help getting a fair understanding of the variationnal formulations of both denoising and segmentation problems, which are presented in Chapter 3 and Chapter 4 respectively. Examples of numerical computations on CT images of the heart are shown for each method. There are many known extensions that are not presented here. Emphasis is put core concepts rather than on technical refinements.

CONTENTS

Abstract	iii
Introduction	1
0.1. The project	1
0.2. The methods	2
Chapter 1. Data	5
1.1. Magnetic Resonance Imaging (MRI)	5
1.2. Computed Tomography (CT)	7
1.3. Visible Human Project	9
Chapter 2. Background	11
2.1. L^p spaces	11
2.2. Radon measures	12
2.3. Approximate continuity	14
2.4. Differentiability	15
2.5. The spaces $BV(\Omega)$ and $SBV(\Omega)$	18
2.6. Calculus of variations	25
Chapter 3. Image denoising	32
3.1. Heat equation	33
3.2. Anisotropic Diffusion	35

3.3. Sobolev smoothing	38
3.4. Total Variation	41
Chapter 4. Segmentation problem	46
4.1. Active Contours (Snake)	46
4.2. Level Set method	47
4.3. Mumford-Shah functional	51
4.4. Piecewise constant Mumford-Shah problem	53
4.5. Active Contour without edges	55
4.6. Numerical results	61
4.6.1. 2D results	62
4.6.2. 3D results	64
4.6.3. Computational remarks	66
Index	69
Bibliography	72

INTRODUCTION

0.1. THE PROJECT

The main goal of this PhD project is to build a precise and complete model of the human heart. This may include:

- (1) An accurate and properly refined mesh of the heart muscle, the cavities, the lungs and the rest of the thorax.
- (2) Information about fine anatomic details such as
 - (a) Orientation of cardiac fibers (which are necessary to perform electrophysiology or mechanical deformation computations),
 - (b) Geometry of the valves (for blood dynamic).

Medical images are about the most reliable source of data on which to base our construction. The challenge is to extract the heart boundaries and other geometrical characteristics from these images. This is called the segmentation process. In a 2D scenario, a human eye can easily detect the contours of objects, then draw these contours. It is quite difficult however to get a computer to do the same thing, but this step is necessary in a 3D context. Indeed, a human would have a lot of trouble to find a boundary surface in 3D images. Moreover, an automation of this process would be a very powerful tool for physicians. Even though automation is not our primary goal, we do favor processes which require little human interaction.

Several PDE-based simulations would benefit from a good heart model:

- (1) Difference of potential computations between the interior and the exterior of the cells which propagates, forcing the contraction of the muscular cells.
- (2) Electrocardiograms simulations.

- (3) Blood flow and mechanical deformations simulations.
- (4) Human organs interaction. A complete model of the thorax and the organs allows for interaction computations.

0.2. THE METHODS

We will focus on PDE-based methods for image analysis. In many cases, the given PDE is the Euler-Lagrange equation of a minimization problem. The solution is the minimum of some function

$$E : V \longrightarrow \mathbb{R},$$

where V is an appropriate vector space.

An image can be seen as a function

$$g : \Omega \subseteq \mathbb{R}^N \longrightarrow [0, 1],$$

where $g(x)$ represents the grey tone of the image at the pixel x . Medical images contain noise, a preprocessing step is therefore necessary before attempting to segment the image.

A celebrated noise removal model is the one proposed by Rudin, Osher and Fatemi [19]. This result states that a function which minimizes the functional

$$E(u) = \int_{\Omega} |\nabla u| dx + \int_{\Omega} (g - u)^2 dx$$

is a clean version of the image g . In order to define the functional E properly, one needs to decide on a space V of admissible functions. This choice must be performed carefully since clean images can contain non trivial discontinuities, and ∇u may not be well defined. For this reason, the space of functions of bounded variations is introduced.

Using a gradient descent method, one deduces that a steady state of the following equation

$$\begin{cases} u_t = \mu \operatorname{div} \left(\frac{\nabla u}{|\nabla u|} \right) + (g - u), & \Omega \\ \frac{\partial u}{\partial n} = 0, & \partial\Omega \\ u(x, 0) = g. \end{cases} \quad (0.2.1)$$

is a local minimum of E .

For the segmentation problem, Mumford and Shah [16] proposed to consider pairs (u, K) , formed of an image u and a compact set of edges K . They state that the pair (u, K) which minimizes

$$F(u, K) = \int_{\Omega \setminus K} |\nabla u|^2 dx + \int_{\Omega} (g - u)^2 dx + \operatorname{length}(K)$$

gives a good segmentation of the image g . In this context, the set K represents the contours of the objects in g . Moreover, the function u should be such that ∇u is well defined on $\Omega \setminus K$. Once again, the use of the space of bounded variations functions is necessary.

It is a difficult task to prove that this functional has indeed a minimum. To compute this minimum numerically, the problem has to be expressed in a simplified form through a level set formulation. This leads to the PDE, proposed by Chan and Vese [6],

$$\begin{cases} \phi_t = \mu \delta(\phi) \left(\operatorname{div} \left(\frac{\nabla \phi}{|\nabla \phi|} \right) + (g - c(\phi)) \right), & \Omega \\ \frac{\partial \phi}{\partial n} = 0, & \partial\Omega \\ \phi(x, 0) = \phi_0, \end{cases} \quad (0.2.2)$$

which is very similar to 0.2.1. The steady state solution splits the domain into two regions, namely $\{\phi < 0\}$ and $\{\phi > 0\}$. These two sets represent regions of interest of the image g . It is then possible to consider one of these regions as a new domain, and split it again. This iterative process gives an efficient way to segment images.

The structure of this report is as follow. In Chapter 1, we briefly talk about the available sources of data, and their acquisition process.

In Chapter 2 we present results from measure theory, functional analysis and calculus of variations required to state and solve the minimisation problems that arise in image processing and image segmentation. This includes main properties of the space of functions of bounded variation, which play a central role in these problems.

In Chapter 3 we present the most popular PDE techniques in image denoising. This is followed in Chapter 4 by the PDE techniques for image segmentation, such as the celebrated Mumford-Shah problem [16] and its simpler version Active Contours without edges [6].

Chapter 1

DATA

Imaging the heart is a difficult task. The main reason for that is this the heart is either constantly moving or, when it is dead, its shape is modified. When the heart beats, the cells contract themselves and make the heart's walls thinner. There are two main types of heart imaging procedures: MRI and CT scans. The Visible Human Project is another source of data but, as the subject is dead, the shape of the heart is unreliable. In all cases, the images are given as series of 2D slices.

1.1. MAGNETIC RESONANCE IMAGING (MRI)

In magnetic resonance imaging, there is a long sequence of operations that are necessary in order to pass from the acquired data to a real image.

Briefly, the process is as follows: The patient is placed into a long thick tube. A strong magnetic field, affecting hydrogen atoms of the body is produced inside the tube. Hydrogen atoms are constituted of a proton and an electron which makes it a dipole. Under the magnetic field, the dipoles all align in the same direction.

A second device, often shaped like a donut, is placed in the scanner around the region of interest. This device also produces a magnetic field that align the hydrogen atoms in a different direction. Everything is then ready for data acquisition: the second magnetic field is stopped and all of a sudden, dipoles come back to their original orientation. When doing so, the atoms release some energy that is captured by the second device. These data are then processed in order

to reconstruct an image representing the hydrogen density. Since hydrogen in the human body mostly comes from water, organs can be colored with respect to their water concentration. This is great for heart imaging. It allows to distinguish between the muscle and the cavities of the heart. Figure 1.1 shows a slice of a typical MRI data set.

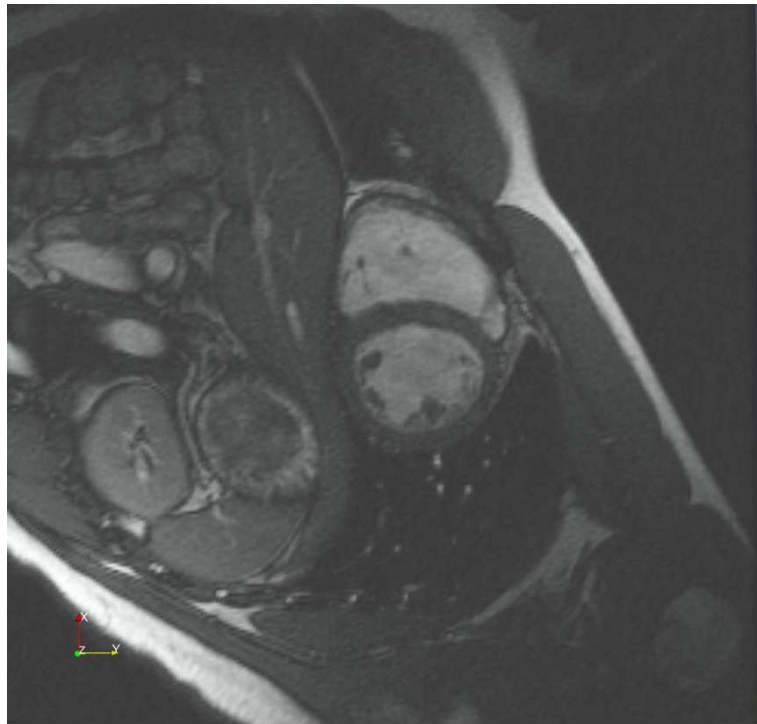


FIG. 1.1. 3D & 4D images of an alive patient, $1.2mm \times 1.2mm \times 6mm$. Courtesy of the *Ontario Consortium of Cardiac Imaging*, Sunnybrook Health Sciences Center, University of Toronto

The MRI data set to which we have access has resolution $1.2mm \times 1.2mm \times 6mm$ and size $256 \times 256 \times 14$.

A drawback of MRI is that to be able to get high resolution data, it takes a long time of acquisition, and during that time, the heart moves. Slices are taken always at the same moment of the beating cycle, usually at the diastole. Then one image is taken at each heart beat. Typically, resolution in the x and

y direction is between 1mm. and 2mm., and the resolution in the z direction between 2mm. and 6mm. This is really bad resolution if ones want to recover fine anatomic details of the heart.

Some MRI scans can actually measure the diffusion of the water in a tissu. The privileged direction for the diffusion of the water is the one of the fibers. This is then a good way to compute the orientation of the cardiac fibers. The downside is that the tissu needs to stay in the scan for a long time, about 50 hours, which is unbearable for a living person.

At Johns Hopkins University, they measured these diffusion tensors from the heart of a dead person. As the heart was dead and it was hanged in some way into the scanner, it does not have a very nice shape. But, this is certainly interesting data since if one has a more realistic model of the heart, it may be possible to reinterpret in some way the data of the fibers on this better model. A picture of a slice can be seen in figure 1.2.

1.2. COMPUTED TOMOGRAPHY (CT)

Computed tomography uses X-ray technology. As for MRI, the patient is placed into a tube. This tube emits X-rays toward the center of the cylinder. They pass through the body and the intensity is measured on the other side. Then a reconstruction work is done to actually obtain a 3D image.

A disadvantage of that method is that it distinguish better bones than organic tissus. It makes a very small difference between the muscle and the cavities of the heart. On the other hand, it offers precise data relatively fast.

The scan always take the pictures at the same moment of the heart beat. It can capture up to 10 slices of 1.2mm per heart beat. On each slice, it is possible to have a resolution of $0.5mm \times 0.5mm.$, which is very good. Figure 1.3 shows a slice of a typical CT scan.

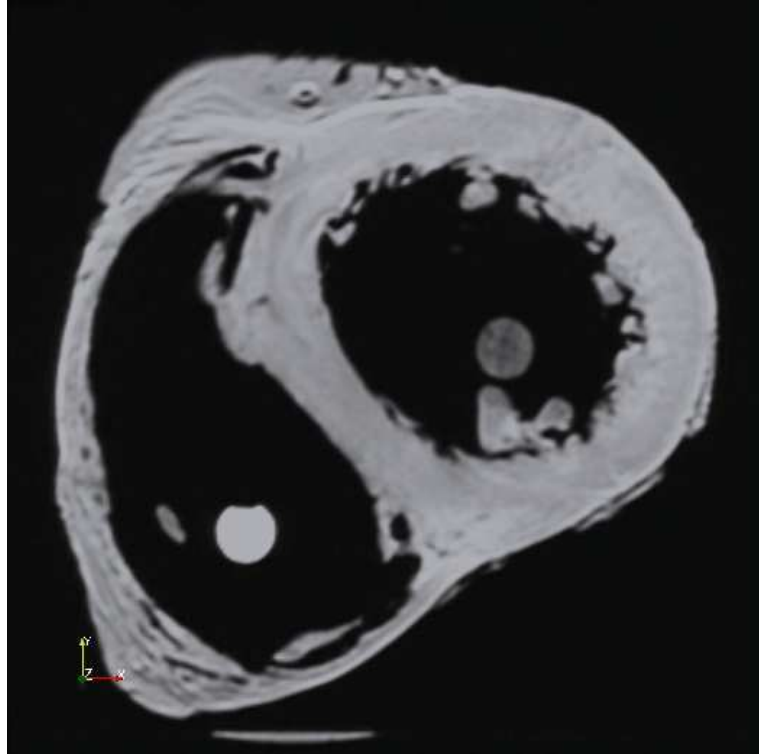


FIG. 1.2. 3D image and fiber information of a dead heart, $0.4mm \times 0.4mm \times 1mm$. The size is $256 \times 256 \times 134$. Courtesy of the Center for Cardiovascular Bio-informatics and Modeling, Johns Hopkins University

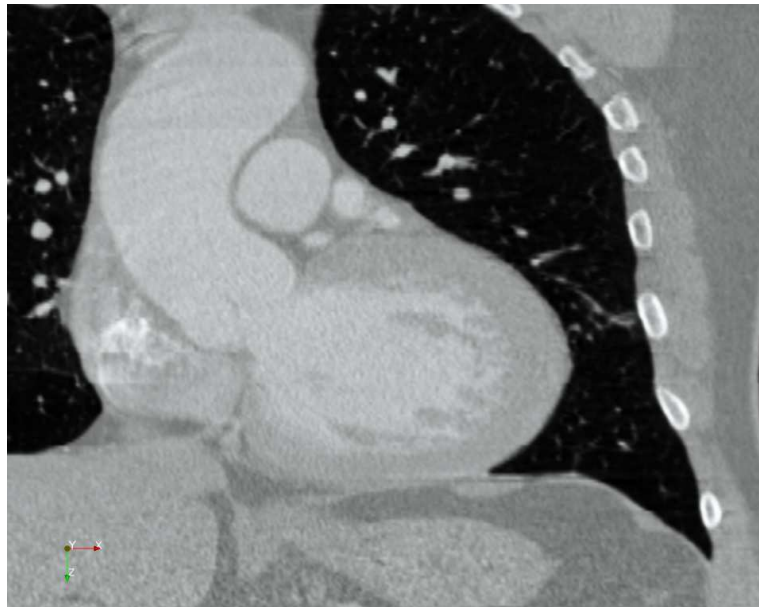


FIG. 1.3. 3D image of an alive patient, $0.5mm \times 0.5mm \times 1.2mm$. Courtesy of the *PET Center*, Heart Institute, University of Ottawa

This CT scan has size $512 \times 512 \times 199$ and is the best data set we have at our hands for the moment.

1.3. VISIBLE HUMAN PROJECT

Another valuable source of data is the one provided by the Visible Human Project. A men and a women (dead) have been frozen in an ice cube. Then they have been thinly sliced ($1mm$ for the men and $0.33mm$) for the women. At each slice, they took a color picture of the result. These data sets are very precise and contain a lot of useful anatomic details. The drawback is that the patient were dead, which changes the shape of the heart. The whole data sets are huge. We selected parts of the thorax around the heart that are shown in figures 1.4 and 1.5. Their sizes are respectively $440 \times 440 \times 121$ and $600 \times 400 \times 381$.

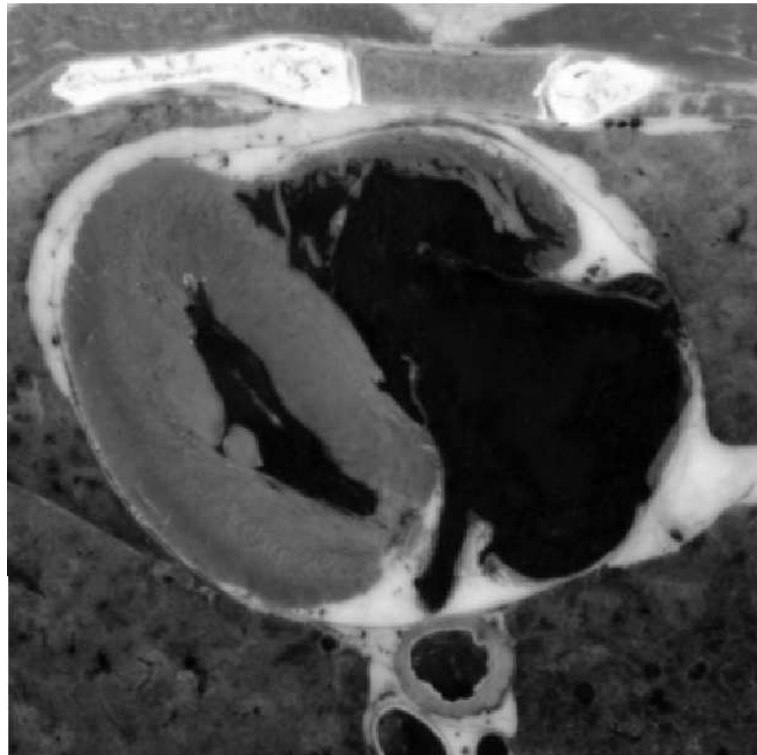


FIG. 1.4. Visible Human Male, $0.33mm \times 0.33mm \times 1mm$. Courtesy of the United States National Library of Medicine

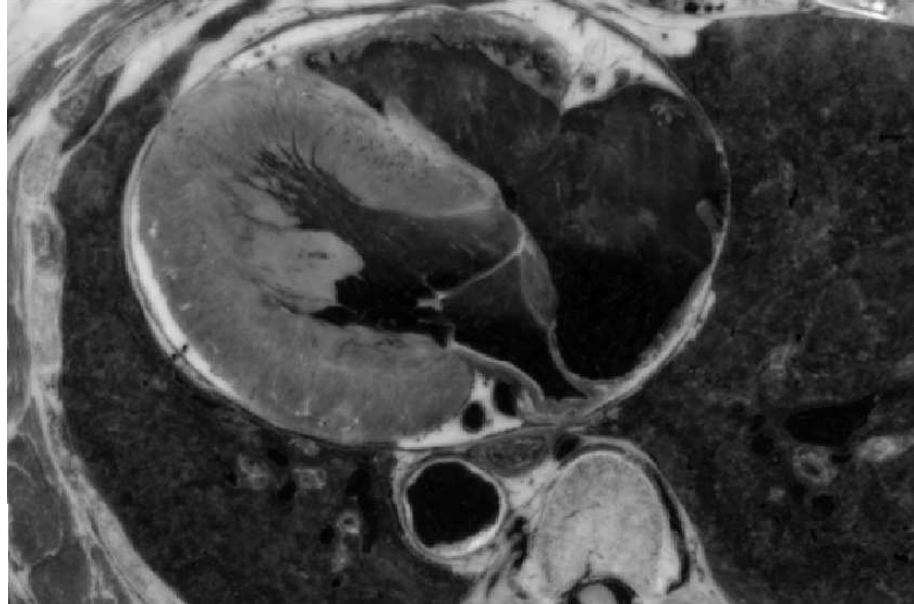


FIG. 1.5. Visible Human Female, $0.33mm \times 0.33mm \times 0.33mm$.
Courtesy of the United States National Library of Medicine

Chapter 2

BACKGROUND

In this chapter, we will present some of the background that is necessary to correctly state and solve variational problems that arise in image de-noising and segmentation. This will contain some measure theory, basic notions about distributions and weak derivatives. For proofs, or more detailed exposition, we recommend for example Rudin ([20] and [21]).

Next, we talk about some fine properties of functions, such as approximate continuity and jump set and introduce spaces of functions of bounded variations, state the main compactness results and go into some proof in order to get a feeling of it. We recommend for this material the excellent and very complete book by Ambrosio ([1]), although there are several other good references such as [9], [25], [4] or [2].

At last, we present some basics of calculus of variations. A more complete treatment can be found for example in Giusti ([10]) or Struwe ([23]).

2.1. L^p SPACES

In this section Ω denotes an open set of \mathbb{R}^N . By $L^p(\Omega)$, we mean $L^p(\Omega, \mathcal{L}^N \llcorner \Omega)$, where \mathcal{L}^N is the Lebesgue measure on \mathbb{R}^N . $u_n \rightharpoonup u$ denotes weak convergence of u_n towards u . Standard theory of L^p spaces is assumed. The statements below are less known and of interest for variational problems in image processing.

Theorem 1. *Let $1 < p < \infty$. If $(u_n)_n \subseteq L^p(\Omega)$ is a bounded sequence, then there exists a subsequence*

$$u_{n_k} \rightharpoonup u \in L^p(\Omega).$$

If $p = 1$, the above theorem is not valid, we need an additional condition on the sequence to ensure the existence of a converging subsequence, namely equiintegrability.

Definition 2. $(u_n)_n \subseteq L^1(\Omega)$ is equiintegrable if and only if

- (1) $\forall \epsilon > 0, \exists A \subseteq \Omega$ such that $\mu(A) < \infty$ and $\forall n, \int_{\Omega \setminus A} u_n dx < \epsilon$,
- (2) $\forall \epsilon > 0, \exists \delta > 0$ such that $\mathcal{L}^N(E) < \delta \Rightarrow \forall n, \int_E |u_n| dx < \epsilon$.

Proposition 3. If Ω is bounded, then $(u_n)_n \subseteq L^1(\Omega)$ is equiintegrable if and only if

$$(u_n)_n \subseteq \left\{ f \in L^1(\Omega) : \int_{\Omega} \phi(|f|) \leq 1 \right\}$$

for some increasing continuous function $\phi : [0, \infty] \rightarrow [0, \infty]$ satisfying $\lim_{t \rightarrow \infty} \phi(t)/t = \infty$.

Theorem 4. A bounded sequence $(u_n)_n \in L^1(\Omega)$ has a weakly convergent subsequence if and only if $(u_n)_n$ is equiintegrable.

2.2. RADON MEASURES

In this section X denotes a locally compact separable metric space.

Definition 5. $\mu : \mathcal{B}(X) \rightarrow \mathbb{R}^N$ is a Radon measure if

- (1) $\mu(\emptyset) = 0$,
- (2) $\forall (E_n)_n \subseteq \mathcal{B}(X)$, pairwise disjoint sets

$$\mu \left(\bigcup_{n=0}^{\infty} E_n \right) = \sum_{n=0}^{\infty} \mu(E_n).$$

The set of all Radon measures on X is denoted $\mathcal{M}(X)$.

Remark 6. For $\mu \in \mathcal{M}(X)$, there is a decomposition $\mu = (\mu_1, \dots, \mu_N)$. For $u \in [C_c(X)]^N$, write

$$\int_X u d\mu = \sum_{i=1}^N \int_X u_i d\mu_i.$$

Definition 7. Let $\mu \in \mathcal{M}(X)$. The total variation of μ

$$|\mu|(E) = \sup \left\{ \sum_{n=0}^{\infty} |\mu E_n| : E_n \in \mathcal{B}(X) \text{ pairwise disjoint, } E = \bigcup_{n=0}^{\infty} E_n \right\}$$

is a finite positive measure on X .

Proposition 8. Let $\mu \in \mathcal{M}(X)$, then for all open set $A \subseteq X$,

$$|\mu|(A) = \sup \left\{ \int_X u d\mu : u \in [C_c(A)]^N, \|u\|_\infty \leq 1 \right\}$$

Remark 9. The set $\mathcal{M}(X)$ is a Banach space when equipped with the norm

$$\|\mu\| = |\mu|(X).$$

The space $\mathcal{M}(X)$ can be identified with the dual of a space of functions. Write $C_0(X)$ for the closure of $C_c(X)$ in the space $C^0(X)$ of continuous functions on X . It corresponds to the continuous functions which vanish at the extremities of X .

Theorem 10 (Riesz). Let

$$L : [C_c(A)]^N \longrightarrow \mathbb{R}$$

be a linear bounded functional. Then there exists a unique $\mu \in \mathcal{M}(X)$ such that

$$\forall \phi \in [C_c(A)]^N, \quad L\phi = \int_X \phi d\mu.$$

Therefore $\mathcal{M}(X) \cong ([C_c(A)]^N)^*$. Moreover

$$\mu(X) = \|L\| = \sup_{\|\phi\|_\infty \leq 1} L(\phi)$$

In view of this fact, it is possible to define a weak* topology on $\mathcal{M}(X)$. This topology turns out to be very useful for applications.

Definition 11. Let $(\mu_n)_n \subseteq \mathcal{M}(X)$. Then $\mu_n \xrightarrow{*} \mu$ if

$$\forall \phi \in [C_c(A)]^N, \quad \int_X \phi d\mu_n \longrightarrow \int_X \phi d\mu.$$

Theorem 12. Let $(\mu_n)_n \in \mathcal{M}(X)$ be such that $\sup_n |\mu_n|(X) < \infty$. Then there exists a subsequence $(\mu_{n_k})_k \xrightarrow{*} \mu \in \mathcal{M}(X)$. Moreover the map $\mu \mapsto |\mu|(X)$ is lower semicontinuous with respect to the weak* convergence. That is

$$\liminf_n |\mu_n|(X) \geq |\mu|(X).$$

Theorem 13. Let $(\mu_n)_n \subseteq \mathcal{M}(\Omega)$ such that $\mu_n \xrightarrow{*} \mu$. If $|\mu_n| \xrightarrow{*} \lambda$, then

$$|\mu| \leq \lambda.$$

Definition 14. Let μ be a positive measure on $\mathcal{B}(X)$, and $\nu \in \mathcal{M}(X)$. Then

(1) ν is absolutely continuous with respect to μ ($\nu \ll \mu$) if

$$\forall E \in \mathcal{B}(X), \quad \mu(E) = 0 \quad \implies \quad \nu(E) = 0.$$

(2) ν and μ are mutually singular ($\nu \perp \mu$) if there exists $E \in \mathcal{B}(X)$ such that

$$\nu(E) = 0 = \mu(E^c).$$

Theorem 15 (Radon-Nikodým). Let μ be a σ -finite measure on $\mathcal{B}(X)$ and $\nu \in \mathcal{M}(X)$. Then there exists $\nu^a, \nu^s \in \mathcal{M}(X)$ such that $\nu^a \ll \mu$, $\nu^s \perp \mu$ and

$$\nu = \nu^a + \nu^s.$$

Moreover, this decomposition is unique and there is a unique $f \in [L^1(X, \mu)]^N$ such that

$$\nu^a = f\mu.$$

Remark 16. If μ and ν are mutually singular, then for any $E \in \mathcal{B}(X)$

$$|\mu + \nu|(E) = |\mu|(E) + |\nu|(E).$$

2.3. APPROXIMATE CONTINUITY

For functions in $L^p(\Omega)$, it is still possible to define some kind of continuity and differentiability.

Definition 17. Let $u \in L^1_{\text{loc}}(\Omega)$. u has an approximate limit at $x \in \Omega$ if there exists $z \in \mathbb{R}$ such that

$$\lim_{\delta \rightarrow 0} \int_{B_\delta(x)} |u(y) - z| dy = 0,$$

where $B_\delta(x)$ denotes the ball of radius δ about x and $\int_B f(x) dx$ denotes the mean value of f over B . If there exists no $z \in \mathbb{R}$ with this property, we say that x is an approximate discontinuity point, and the approximate discontinuity set S_u is the

set of such points. u has an approximate jump at $x \in \Omega$ if there exists $z^+, z^- \in \mathbb{R}$ such that

$$\lim_{\delta \rightarrow 0} \int_{B_\delta^+(x)} |u(y) - z^+| dy = 0 = \lim_{\delta \rightarrow 0} \int_{B_\delta^-(x)} |u(y) - z^-| dy,$$

where B_δ^\pm denote half balls of radius δ about x . J_u is the set of such points is the jump set. Then $J_u \subseteq S_u$.

The following theorem gather facts about S_u and J_u are important.

Theorem 18. *Let $u \in L^1_{\text{loc}}(\Omega)$. Then*

- (1) $\mathcal{L}^N(S_u) = 0$,
- (2) $\mathcal{H}^{N-1}(S_u \setminus J_u) = 0$,

where \mathcal{H}^{N-1} stands for the $(N - 1)$ -dimensional Hausdorff measure.

2.4. DIFFERENTIABILITY

Definition 19. *Let $\mathcal{D}(\Omega)$ be the set of C^∞ functions with compact support in Ω . Then provide $\mathcal{D}(\Omega)$ the following topology: we say that $\phi_n \xrightarrow{\mathcal{D}(\Omega)} \phi$ if there exists a compact $K \in \Omega$ such that for all n , $\text{spt}\phi_n \subseteq K$ and for all $\alpha \in \mathbb{N}^N$, $D^\alpha \phi_n$ converge uniformly to $D^\alpha \phi$ on K .*

Remark 20. *The space $\mathcal{D}(\Omega)$ cannot be equipped with a norm. It has in fact a sequence of semi-norms, namely the C^k norms.*

Definition 21. *The space of distributions $\mathcal{D}'(\Omega)$ is the dual of $\mathcal{D}(\Omega)$, ie*

$$\mathcal{D}'(\Omega) = \{L : \mathcal{D}(\Omega) \longrightarrow \mathbb{R} : L \text{ is a continuous linear functionnal}\}.$$

It is common to write $(L, \phi)_{\mathcal{D}(\Omega)}$ (or simply (L, ϕ)) for $L\phi$.

Example 22. *Given $f \in L^1$, define the distribution*

$$L_f : \mathcal{D}(\Omega) \longrightarrow \mathbb{R},$$

$$\phi \mapsto (f, \phi)_{\mathcal{D}(\Omega)} = \int_{\Omega} f \phi dx.$$

Suppose f is C^1 , then by Green's theorem and the fact that $\phi|_{\partial\Omega} = 0$

$$(D_i f, \phi)_{\mathcal{D}(\Omega)} = \int_{\Omega} D_i f \phi \, dx = - \int_{\Omega} f D_i \phi \, dx = -(f, D_i \phi)_{\mathcal{D}(\Omega)},$$

which suggests:

Definition 23. The partial derivative of a distribution L in the direction x_i is

$$\begin{aligned} D_i L : \mathcal{D}(\Omega) &\longrightarrow \mathbb{R}, \\ \phi &\longmapsto -(L, D_i \phi)_{\mathcal{D}(\Omega)}. \end{aligned}$$

The total derivative of L is $DL = (D_1 L, \dots, D_N L)$. For $\phi \in [\mathcal{D}(\Omega)]^N$, we write

$$(DL, \phi)_{[\mathcal{D}(\Omega)]^N} = (DL_1 \phi_1)_{\mathcal{D}(\Omega)} + \dots + (DL_N \phi_N)_{\mathcal{D}(\Omega)}.$$

Hence remark that

$$(DL, \phi)_{[\mathcal{D}(\Omega)]^N} = -(L, \operatorname{div} \phi)_{\mathcal{D}(\Omega)}.$$

Definition 24 (Sobolev functions). Let $f \in L^p(\Omega)$. We say that f belongs to the Sobolev space $W^{1,p}(\Omega)$ if its total derivative Df in the sense of distributions belongs to $[L^p(\Omega)]^N$. Which means that there exists $g \in [L^p(\Omega)]^N$ such that

$$\forall \phi \in [\mathcal{D}(\Omega)]^N \quad - \int_X f \operatorname{div} \phi \, dx = \int_X g \cdot \phi \, dx.$$

$W^{1,p}(\Omega)$ is a Banach space with the norm

$$\|f\|_{W^{1,p}(\Omega)}^p = \|f\|_{L^p}^p + \sum_i \|D_i f\|_{L^p(\Omega)}^p.$$

$W^{1,2}(\Omega)$ is even a Hilbert space with the dot product

$$(f, g)_{W^{1,2}(\Omega)} = (f, g)_{L^2(\Omega)} + \sum_i (D_i f, D_i g)_{L^2(\Omega)},$$

and is often denoted by $H^1(\Omega)$.

Definition 25 (Functions of bounded variation). $f \in L^1$ is of bounded variation if there exists a finite signed measure μ such that

$$\forall \phi \in [\mathcal{D}(\Omega)]^N, \quad - \int_{\Omega} f \operatorname{div} \phi \, dx = \int_{\Omega} \phi \, d\mu.$$

Write $BV(\Omega)$ for the space of functions of bounded variation and $Df = \mu = (\mu_1, \dots, \mu_N)$ is the total derivative of f in the sense of distributions. The measure μ_i is the partial derivative of u in the direction x_i . The space $BV(\Omega)$ is a Banach space with the norm

$$\|f\|_{BV(\Omega)} = \|f\|_{L^1} + |Df|(X),$$

where $|Df|$ is the total variation of the Radon measure Df .

Remark 26. Let $u \in BV(\Omega)$ and $\mu = Du$. Then by Riez theorem,

$$|\mu|(E) = \sup_{\substack{\phi \in \mathcal{D}(\Omega) \\ \|\phi\|_\infty \leq 1}} \int_E u \operatorname{div} \phi \, dx = \sup_{\substack{\phi \in \mathcal{D}(\Omega) \\ \|\phi\|_\infty \leq 1}} \int_E \phi d\mu \, dx.$$

Example 27. Let $u : (-1, 1) \rightarrow \mathbb{R}$ be the function

$$u(x) = \begin{cases} 0, & x \leq 0, \\ x^2/2, & x > 0. \end{cases}$$

Therefore

$$u'(x) = \begin{cases} 0, & x \leq 0, \\ x, & x > 0. \end{cases} \quad u''(x) = \begin{cases} 0, & x \leq 0, \\ 1, & x > 0. \end{cases} \quad u'''(x) = \delta$$

Then we have

$$\begin{aligned} u' \in C^0(-1, 1) &\implies u \in C^1(-1, 1) \\ u'' \in L^1(-1, 1) &\implies u' \in W^{1,1}(-1, 1) \\ u''' = \delta \in \mathcal{M}(-1, 1) &\implies u' \in BV(-1, 1). \end{aligned}$$

Example 28. Let $E \subseteq \Omega$. Define the perimeter of E in Ω to be

$$P(E, \Omega) = |D\chi_E|(\Omega).$$

It is said that E is of finite perimeter in Ω if $P(E, \Omega) < \infty$. Now suppose ∂E is C^1 . Then by Gauss-Green theorem and proposition 8,

$$\begin{aligned} |D\chi_E|(\Omega) &= \sup_{\substack{\phi \in \mathcal{D}(\Omega) \\ \|\phi\|_\infty \leq 1}} \int_{\Omega} \phi dD\chi_E = \sup_{\substack{\phi \in \mathcal{D}(\Omega) \\ \|\phi\|_\infty \leq 1}} \int_{\Omega} \operatorname{div} \phi \chi_E dx \\ &= \sup_{\substack{\phi \in \mathcal{D}(\Omega) \\ \|\phi\|_\infty \leq 1}} \int_E \operatorname{div} \phi dx = \sup_{\substack{\phi \in \mathcal{D}(\Omega) \\ \|\phi\|_\infty \leq 1}} \int_{\partial E \cap \Omega} \phi \cdot \nu d\mathcal{H}^{N-1} = \mathcal{H}^{N-1}(\partial E \cap \Omega). \end{aligned}$$

The last equality seems obvious, but requires some work. The result is still true in a more general context: If E has finite perimeter, then

$$P(E, \Omega) = \mathcal{H}^{N-1}(\partial E \cap \Omega).$$

2.5. THE SPACES $BV(\Omega)$ AND $SBV(\Omega)$

In this section Ω denotes a bounded open set of \mathbb{R}^N with Lipschitz boundary. It turns out that the $BV(\Omega)$ -norm is too strong for most of the applications. The weak* convergence is then very useful.

Definition 29. Let $(u_n)_n \subseteq BV(\Omega)$. Then $u_n \xrightarrow{*} u \in BV(\Omega)$ if

- (1) $u_n \xrightarrow{L^1(\Omega)} u$, and
- (2) $Du_n \xrightarrow{*} Du$ as Radon measures.

It has the following nice properties:

Theorem 30. Let $(u_n)_n \subseteq BV(\Omega)$ and $u \in BV(\Omega)$. Then

$$u_n \xrightarrow{*} u \iff u_n \xrightarrow{L^1(\Omega)} u \quad \text{and} \quad \sup_n \|u_n\|_{BV(\Omega)} < \infty.$$

Theorem 31 (Compactness in $BV(\Omega)$). Let $(u_n)_n \subseteq BV(\Omega)$ be such that

$$\sup_n \|u_n\|_{BV(\Omega)} < \infty,$$

then there exists $u \in BV(\Omega)$ and a subsequence u_{n_k} such that $u_{n_k} \xrightarrow{*} u$.

Using Radon-Nikodým theorem, there exists a unique $g \in [L^1(\Omega)]^N$ such that

$$Du = D^a u + D^s u = g \mathcal{L}^N + D^s u.$$

So for $\phi \in [\mathcal{D}(\Omega)]^N$,

$$\int_{\Omega} f \operatorname{div} \phi \, dx = \int_X g \phi \, dx + \int_{\Omega} \phi dD^s u.$$

This suggest the notation $\nabla u = g$, which represents the Sobolev part of derivative Du of the function u .

Theorem 32 (Decomposition of derivatives). *Let $u \in BV(\Omega)$, then*

$$Du = D^a u + D^j u + D^c u = g \mathcal{L}^N + (u^+ - u^-) \nu_u \mathcal{H}^{N-1} \llcorner J_u + D^c.$$

Where J_u is the set of approached discontinuities of u , ν_u is a normal vector to the discontinuity set, \mathcal{H}^{N-1} is the Hausdorff measure and u^+ , u^- stand for the limits of u on both sides of J_u . $D^j u$ is the jump part of the function u . $D^c u$ is called the Cantor part and has Hausdorff dimension $d \in (N - 1, N)$.

Remark 33. *The notation $D^c u$ is motivated by the fact that the Cantor-Vitali function $u \in BV(0, 1)$ is such that $Du = D^c u$ and $\operatorname{supp} Du$ is included in the Cantor set. We will consider functions that don't have derivatives of this type.*

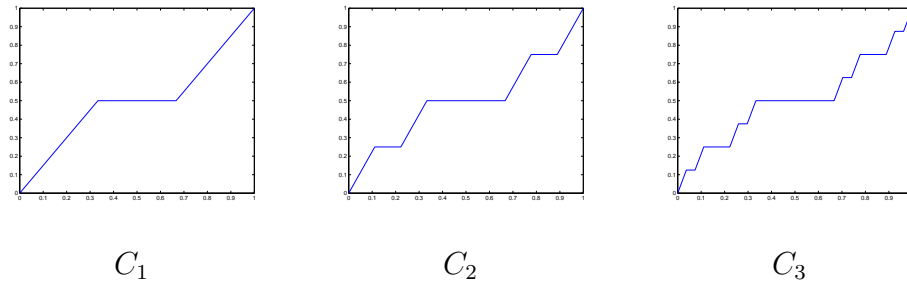


FIG. 2.1. The Cantor-Vitali function C is the limit of the above sequence of functions. It is continuous, monotonely increasing, $|Du|(0, 1) = 1$, but $C' = 0$ almost everywhere. In fact, the support of DC is exactly the Cantor set.

Remark 34. *Let $u \in BV(\Omega)$, then $|Du|(\Omega) < \infty$. From remark 16, it follows that*

$$|Du|(\Omega) = |\nabla u \mathcal{L}^N|(\Omega) + |D^s u|(\Omega) < \infty.$$

Hence both terms on the right side are finite.

Definition 35 (Special functions of bounded variation). *Let $u \in BV(\Omega)$, then $u \in SBV(\Omega)$ if $D^c u = 0$. Or equivalently $u \in SBV(\Omega)$ if and only if $D^s u$ has support in a measurable σ -finite set with respect to \mathcal{H}^{N-1} .*

Example 36. *Let $u_1, u_2 \in W^{1,1}(\Omega) \cap L^\infty(\Omega)$ and $E \in \Omega$ a subset of finite perimeter in Ω . Then*

$$u = u_1 \chi_E + u_2 \chi_{\Omega \setminus E} \in SBV(\Omega).$$

Example 37. *An image is some function $g : \Omega \rightarrow \mathbb{R}$, that is smooth inside the boundaries of the objects and discontinuous on their boundary which have \mathcal{H}^{N-1} -finite measure. If $\|g\|_\infty < \infty$, then $g \in SBV(\Omega)$.*

Proposition 38. *The space $SBV(\Omega)$ is closed with respect to the $BV(\Omega)$ norm.*

PROOF. Let $u_n \xrightarrow{BV(\Omega)} u$. If Du_n is concentrated on B_n which is σ -finite with respect to \mathcal{H}^{N-1} , then by the fact that $|D(u_n - u)| \rightarrow 0$, we have that Du is concentrated on $\cup_n B_n$, which is σ -finite with respect to \mathcal{H}^{N-1} . \square

However the closure of $SBV(\Omega)$ with respect to the weak* convergence would be more interesting. In fact $SBV(\Omega)$ is not closed with respect to the weak* topology, but it is possible to find sufficient conditions for the limit of a sequence of functions in $SBV(\Omega)$ to be in $SBV(\Omega)$. These will come from the following result about chain rule in $BV(\Omega)$.

Theorem 39 (Chain rule in $BV(\Omega)$). *Let $u \in BV(\Omega)$ and $\psi \in C^1(\mathbb{R})$ such that $\psi(0) = 0$, then $\psi \circ u \in BV(\Omega)$ and*

$$D(\psi \circ u) = \psi'(u) \nabla u \mathcal{L}^N + (\psi(u^+) - \psi(u^-)) \nu_u \mathcal{H}^{N-1} \llcorner J_u + \psi'(\tilde{u}) D^c u,$$

where \tilde{u} denotes the approximate limit of u . If Ω is bounded, then the hypothesis $\psi(0) = 0$ can be removed.

So if $u \in SBV(\Omega)$, for all $\psi \in C^1(\mathbb{R}) \cap W^{1,\infty}(\mathbb{R})$, we have

$$\begin{aligned} |D\psi(u) - \psi'(u)\nabla u\mathcal{L}^N| &= |(\psi(u^+) - \psi(u^-))\nu_u\mathcal{H}^{N-1}\llcorner J_u| \\ &\leq 2\|\psi\|_\infty|D^j u|. \end{aligned}$$

Where $\nu \leq \mu$ as measures means that for every measurable set E , we have $\nu(E) \leq \mu(E)$. It turns out that the reverse holds in the following sense:

Theorem 40. *Let $u \in BV(\Omega)$. If there exists $a \in [L^1(\Omega)]^N$ and μ a finite positive measure on Ω such that $\forall \psi \in C^1(\mathbb{R}) \cap W^{1,\infty}(\mathbb{R})$*

$$|D\psi(u) - \psi'(u)a\mathcal{L}^N| \leq \|\psi\|_\infty\mu,$$

then $u \in SBV(\Omega)$. Moreover $a = \nabla u$ and $\mu \geq \mathcal{H}^{N-1}\llcorner J_u$.

It is then possible to prove the following closure property of $SBV(\Omega)$.

Theorem 41 (Closure of $SBV(\Omega)$). *Let $\Omega \subseteq \mathbb{R}^N$ be a bounded domain and $(u_n)_n \subseteq SBV(\Omega)$ such that $u_n \xrightarrow{*} u \in BV(\Omega)$ and*

$$\sup_n \left\{ \int_\Omega |\nabla u_n|^2 dx + \mathcal{H}^{N-1}(J_{u_n}) \right\} < \infty.$$

Then $u \in SBV(\Omega)$ and

- (1) $\nabla u_n \rightharpoonup \nabla u$ in $[L^1(\Omega)]^N$,
- (2) $D^j u_n \xrightarrow{*} D^j u$.

Moreover

$$\int_\Omega |\nabla u|^2 dx \leq \liminf_n \int_\Omega |\nabla u_n|^2 dx$$

and

$$\mathcal{H}^{N-1}(J_u) \leq \liminf_n \mathcal{H}^{N-1}(J_{u_n}).$$

PROOF. Note that

$$Du_n = \nabla u_n \mathcal{L}^N + D^j u_n \xrightarrow{*} Du.$$

One need to show that $\nabla u_n \rightharpoonup \nabla u$, $D^j u_n \xrightarrow{*} D^j u$ and $D^c u = 0$.

First take a look at the jump part. By hypothesis, if $\mu_n = \mathcal{H}^{N-1}\llcorner J_{u_n}$, then

$$\sup_n \mu_n(X) = \sup_n \mathcal{H}^{N-1}(J_{u_n}) < \infty.$$

Therefore by compactness of $\mathcal{M}(\Omega)$ (theorem 12), we can suppose that

$$\mu_n \xrightarrow{*} \mu \in \mathcal{M}(\Omega) \text{ (up to a subsequence).}$$

For the absolutely continuous part, note that

$$\sup_n \int_{\Omega} |\nabla u_n|^2 dx < \infty.$$

Since Ω is bounded, proposition 3 with $\phi(t) = t^2$ ensure equiintegrability of (∇u_n) . Therefore by theorem 4, it has a weakly convergent subsequence (denoted again ∇u_n). So

$$\nabla u_n \rightharpoonup a \in [L^1(\Omega)]^N.$$

ie $\forall g \in [L^\infty(\Omega)]^N, \int_{\Omega} \nabla u_n \cdot g dx \longrightarrow \int_{\Omega} a \cdot g dx$. Therefore $\nabla u_n \mathcal{L}^N \rightharpoonup a \mathcal{L}^N$ in the sense of Radon measures. Theorem 40 is used to establish that $a = \nabla u$ and $\mu \geq D^j u$. Let $\psi \in W^{1,\infty}(R) \cap C^1(\mathbb{R})$. First note that

$$\psi'(u_n) \nabla u_n \rightharpoonup \psi'(u) a.$$

Indeed, let $\epsilon > 0$ and $\delta > 0$ be such that $|x-y| < \delta \Rightarrow |\psi'(x) - \psi'(y)| < \epsilon/2 \mathcal{L}^N(\Omega)$. Now since $u_n \xrightarrow{L^1(\Omega)} u$, u_n converges in measure to u , and then there exists a $M > 0$ such that

$$n \geq M \Rightarrow \mathcal{L}^N(\{x : |u_n(x) - u(x)|^2 > \delta\}) < \frac{\epsilon}{4\|\psi'\|_{\infty}}.$$

Set $A_{\delta} = \{x : |u_n(x) - u(x)|^2 > \delta\}$, then

$$\begin{aligned} \int_{\Omega} |\psi'(u_n) - \psi'(u)| dx &= \int_{A_{\delta}} |\psi'(u_n) - \psi'(u)| dx + \int_{A_{\delta}^c} |\psi'(u_n) - \psi'(u)| dx \\ &\leq 2\|\psi'\|_{\infty} \mathcal{L}^N(A_{\delta}) + \mathcal{L}^N(A_{\delta}^c) \frac{\epsilon}{2\mathcal{L}^N(\Omega)} \leq \epsilon/2 + \epsilon/2 = \epsilon. \end{aligned}$$

So $\psi'(u_n) \xrightarrow{L^2(\Omega)} \psi'(u)$. For any $g \in L^\infty(\Omega)$,

$$\int_{\Omega} \psi'(u_n) \nabla u_n g dx = \int_{\Omega} \nabla u_n g (\psi'(u_n) - \psi'(u)) dx + \int_{\Omega} \nabla u_n (\psi'(u) g) dx.$$

But by Cauchy-Schwartz inequality

$$\int_{\Omega} \nabla u_n g (\psi'(u_n) - \psi'(u)) dx \leq \|\nabla u_n g\|_{L^2(\Omega)} \|\psi'(u_n) - \psi'(u)\|_{L^2(\Omega)} \longrightarrow 0,$$

since $\|\nabla u_n g\|_{L^2(\Omega)}$ is bounded. Also since $\psi'(u)g \in L^\infty(\Omega)$,

$$\int_{\Omega} \nabla u_n(\psi'(u)g) dx \longrightarrow \int_{\Omega} a\psi'(u)g dx.$$

Hence $\forall g \in L^\infty(\Omega)$,

$$\int_{\Omega} \psi'(u_n)\nabla(u_n)g dx \longrightarrow \int_{\Omega} a\psi'g dx,$$

ie $\psi'(u_n)\nabla u_n \rightharpoonup \psi'(u)a$.

From theorem 39 (chain rule formula), it is clear that

$$\sup_n \|u_n\|_{BV(\Omega)} < \infty \implies \sup_n \|\psi(u_n)\|_{BV(\Omega)} < \infty.$$

Moreover $\psi(u_n) \xrightarrow{L^1(\Omega)} \psi(u)$, so by theorem 30, $\psi(u_n) \overset{*}{\rightharpoonup} \psi(u)$, ie. $D\psi(u_n) \overset{*}{\rightharpoonup} D\psi(u)$, which implies that

$$D\psi(u_n) - \psi'(u_n)\nabla u_n \mathcal{L}^N \overset{*}{\rightharpoonup} D\psi(u) - \psi'(u)a \mathcal{L}^N.$$

What is needed is a relation between the absolute values of these measures. Note that

$$\sup_n |D\psi(u_n) - \psi'(u_n)\nabla u_n \mathcal{L}^N|(\Omega) = \sup_n |D^s \psi(u_n)|(\Omega) \leq \sup_n |D\psi(u_n)|(\Omega) < \infty.$$

Hence, there is a subsequence (that may depend on ψ) such that

$$D\psi(u_{n_k}) - \psi'(u_{n_k})\nabla u_{n_k} \mathcal{L}^N \overset{*}{\rightharpoonup} \lambda.$$

Hence theorem 13 asserts that

$$|D\psi(u) - \psi'(u)a \mathcal{L}^N| \leq \lambda.$$

Now for every $k \geq 0$

$$\begin{array}{ccc} |D\psi(u_{n_k}) - \psi'(u_{n_k})\nabla u_{n_k} \mathcal{L}^N| & \leq & 2\|\psi\|_{\infty} \mu_{n_k} \\ \Big\|_* & & \Big\|_* \\ \lambda & \leq & 2\|\psi\|_{\infty} \mu \end{array}$$

since weak* convergence preserves inequalities. Therefore

$$|D\psi(u) - \psi'(u)a \mathcal{L}^N| \leq \lambda \leq 2\|\psi\|_{\infty} \mu.$$

Then by theorem 40, $u \in SBV(\Omega)$. Moreover $a = \nabla u$ and $\mu \geq \mathcal{H}^{N-1} \llcorner J_u$. Hence

$$\nabla u_n \mathcal{L}^N \xrightarrow{*} \nabla u \mathcal{L}^N \quad \text{and} \quad D^j u_n = Du_n - \nabla u_n \mathcal{L}^N \xrightarrow{*} Du - \nabla u \mathcal{L}^N = D^j u.$$

The inequality

$$\int_{\Omega} |\nabla u|^2 dx \leq \liminf_n \int_{\Omega} |\nabla u_n|^2 dx$$

will follow from the lower semi-continuity of the functional $v \mapsto \int_{\Omega} |v|^2 dx$ on $L^2(\Omega)$, which is guaranteed by theorem 55 below.

Finally,

$$\mathcal{H}^{N-1}(J_u) \leq \mu(J_u) \leq \mu(X) \leq \liminf_n \mu_n(X) = \liminf_n \mathcal{H}^{N-1}(J_{u_n}),$$

where the inequality $\mu(X) \leq \liminf_n \mu_n(X)$ comes from lower semi-continuity of total variation of Radon measures (see theorem 12) \square

Theorem 42 (Compactness in $SBV(\Omega)$). *Let $\Omega \subseteq \mathbb{R}^N$ be a bounded domain and $(u_n)_n \subseteq SBV(\Omega)$ such that $\sup_n \|u_n\|_{\infty} < \infty$ and*

$$\sup_n \left\{ \int_{\Omega} |\nabla u_n|^2 dx + \mathcal{H}^{N-1}(J_{u_n}) \right\} < \infty.$$

Then there exists a subsequence $u_{n_k} \xrightarrow{} u \in SBV(\Omega)$.*

PROOF. It is sufficient to show that $\sup_n \|u_n\|_{BV} < \infty$ and apply theorem 31 to obtain a converging subsequence $u_{n_k} \xrightarrow{*} u$.

First note that

$$\sup_n \|u_n\|_{L^1(\Omega)} = \sup_n \int_{\Omega} |u_n| dx \leq \sup_n \|u_n\|_{\infty} \mathcal{L}^N(\Omega) < \infty.$$

Also

$$\begin{aligned} \sup_n |Du_n|(\Omega) &= \sup_n \left\{ \int_{\Omega} |\nabla u_n| dx + \int_{J_{u_n}} |u_n^+ - u_n^-| dx \right\} \\ &\leq \sup_n \left\{ \int_{\Omega} (|\nabla u_n|^2 + 1) dx + 2\|u_n\|_{\infty} \mathcal{H}^{N-1}(J_{u_n}) \right\} \\ &\leq \sup_n \left\{ \int_{\Omega} |\nabla u_n|^2 dx + \mathcal{L}^N(\Omega) + 2\|u_n\|_{\infty} \mathcal{H}^{N-1}(J_{u_n}) \right\} < \infty. \end{aligned}$$

Therefore $\sup_n \|u_n\|_{BV(\Omega)} < \infty$ as needed. \square

2.6. CALCULUS OF VARIATIONS

In the Calculus of Variations, one tries to determine the existence of some critical points. Historically, mathematicians were interested in minima, since the functionals of interest were deduced from laws of physics where the critical points represent “real” physical solutions.

Definition 43. *Let E be a Banach space and $F : V \rightarrow \mathbb{R}$ be a continuous functional. The problem*

$$\inf_{u \in V} F(u) \tag{2.6.1}$$

is a minimisation problem. The goal is to determine the existence and the possible unicity of a solution.

If it is possible to define a derivative for F , it is natural to think that at a minimum u^*

$$DF(u^*) = 0.$$

This is the *Euler-Lagrange equation* of the functional F . This gives a necessary condition for u^* being a local minimum. Note that *a priori* $DF(u^*) = 0$ only implies that u^* is a critical point of F . It can be minimum, a maximum or a saddle point. Even, if it is a minimum, it may be only a local one.

Example 44. *Let $\Omega \subseteq \mathbb{R}$, $V = \{u \in C^1(\Omega) : u|_{\partial\Omega} = h\}$ and*

$$F : V \rightarrow \mathbb{R}$$

$$u \mapsto \int_{\Omega} L(x, u, u'),$$

where $L : \Omega \times \mathbb{R} \times \mathbb{R}$ is a C^2 function. Suppose u is a minimum for F . Then for any $\phi \in C_0^\infty(\Omega)$, $g_\phi(t) = u + t\phi \in E$, and the real function

$$t \mapsto F(g_\phi(t))$$

has a critical point at $t = 0$. Using differentiation, integration by parts and the fact that this is valid for all ϕ , everything boils down to the Euler-Lagrange

equation of F :

$$\frac{\partial L}{\partial u} - \frac{\partial}{\partial x} \left(\frac{\partial L}{\partial u'} \right) = 0.$$

In general, if E is a space of functions, the Euler-Lagrange equation $DF = 0$ will have the form of a partial differential equation. A classical idea is that if you follow the gradient flow, you must end at a critical point, ie. a solution of the Euler-Lagrange equation (under some compactness assumptions). Since minimums are of great interest, one consider flow lines in the directions of the negative gradient. These are given by the partial differential equation $u_t = -DF(u)$. Therefore, to find a local minimum, one picks an initial function u_0 , and solve the problem

$$\begin{cases} u_t = -DF(u), \\ u(x, 0) = u_0 \end{cases}$$

iteratively to obtain a sequence u_n that could converge to a local minimum. This approach is very convenient to find explicitly a critical point. Note that if we can prove the convergence of such an algorithm, then using numerical computations, there is no choice that to end at a local minimum, since other critical points are unstable, however the minimum may not be the global minimum. An important issue is the one of the existence of a solution, that will ensure that the sequence f_n converges. A standard way to tackle the existence problem is to use the direct method.

Definition 45. *To solve (2.6.1) by the direct method, first pick a minimizing sequence $(x_n)_n$, i.e.*

$$\lim_{n \rightarrow \infty} x_n = \inf_{x \in E} F(x) = c.$$

Then choose a suitable topology τ on E , in the sense that the following steps are feasible.

(1) *Show that (x_n) admits a convergent subsequence*

$$x_{n_k} \xrightarrow{\tau} x$$

for the topology τ .

(2) Show that

$$F(x) = c.$$

(This step is non trivial because F may not be continuous with respect to τ .)

The way to achieve this highly depends on the space E and on the functional F . A common hypothesis is coercivity.

Definition 46. A fonction $F : E \rightarrow \mathbb{R}$ is coercive if

$$\lim_{|x|_E \rightarrow \infty} F(x) = \infty.$$

Proposition 47. Let $F : \mathbb{R}^n \rightarrow \mathbb{R}$ be continuous and coercive. Then the problem

$$\inf_{x \in E} F(x)$$

admits a solution.

PROOF. Let $(x_n)_n$ be a minimising sequence. By coercivity $(x_n)_n$ is bounded. It admits a converging subsequence $x_{n_k} \rightarrow x$ for the usual topology. Then

$$F(x) = F\left(\lim_{n_k} x_{n_k}\right) = \lim_{n_k} F(x_{n_k}) = \inf_{x \in E} F(x).$$

□

In many case, it is too restrictive to consider only continuous functions. We can relax this assumption by considering lower-semi-continuous functions.

Definition 48. F is τ -lower-semi-continuous (l.s.c.) if

$$\forall x_n \xrightarrow{\tau} x, \quad \liminf_n F(x_n) \geq F(x).$$

Equivalently

$$f \text{ is l.s.c.} \quad \Leftrightarrow \quad \forall c \in \mathbb{R}, \{F > c\} \text{ is open}$$

Remark 49. If $E = \mathbb{R}^n$ and τ denotes the usual topology on \mathbb{R}^n , then

$$F \text{ is l.s.c. and coercive} \quad \Leftrightarrow \quad \forall c \in \mathbb{R}, E_c = \{F \leq c\} \text{ is compact.}$$

Proposition 50. *Let $F : \mathbb{R}^n \rightarrow \mathbb{R}$ be l.s.c. and coercive. Then the problem*

$$\inf_{x \in E} F(x)$$

admits a solution.

PROOF. Let $(x_n)_n$ be a minimising sequence and $c_n = F(x_n)$. Then

$$E_{c_0} \supseteq E_{c_1} \supseteq E_{c_2} \supseteq \dots$$

is a decreasing sequence of compacts. There must exist $x \in E$ that belongs to each E_{c_n} , which leads to

$$\forall n, \quad F(x) \leq c_n.$$

□

In these examples, it has not been necessary to pick an other topology because the space E was of finite dimension. But it appears that in most situations, a weaker topology is needed. Indeed, if the functional is coercive, then minimizing sequences are bounded, but in general one cannot hope that a bounded sequence admits a convergent subsequence. Hence, it is necessary to choose a coarser topology τ , that has bigger compacts. At the same time τ must be fine enough to have lower semicontinuity of F .

Theorem 51. *Let E be a reflexive Banach space (that is $E^{**} = E$). Then a bounded sequence $(x_n)_n$ in E admits a weakly convergent subsequence*

$$x_{n_k} \rightharpoonup x.$$

This leads to

Theorem 52. *Let E be a reflexive Banach space and $F : E \rightarrow \mathbb{R}$ be a coercive functional, which is weakly l.s.c., then the problem*

$$\inf_x F(x)$$

admits a solution.

Weak l.s.c. may be hard to prove. The following criterion is often used.

Theorem 53. Let $F : E \rightarrow \mathbb{R}$ be a convex functionnal, then

$$F \text{ is l.s.c.} \quad \Leftrightarrow \quad F \text{ is weakly l.s.c.}$$

Then Theorem 52 becomes

Theorem 54. Let E be a reflexive Banach space and

$$F : E \rightarrow \mathbb{R}$$

be a coercive convex l.s.c. functionnal, then the problem

$$\inf_x F(x)$$

admits a solution.

But this result does not hold for functionals on $L^1(\Omega)$, since it is not a reflexive space. It is possible to prove the following results for functional on $L^1(\Omega)$.

Theorem 55. Let $F(x, u) : \Omega \times \mathbb{R}^s \rightarrow \bar{\mathbb{R}}$ be a C^1 function and $u_n, u \in L^1(\Omega)$. If one of the following holds

$$(1) u_n \xrightarrow{L^1(\Omega)} u \text{ or}$$

$$(2) u_n \xrightarrow{L^1(\Omega)} u \text{ and for all } x \in \Omega, \text{ the function } F(x, \cdot) \text{ is convex,}$$

then

$$\int_{\Omega} F(x, u(x)) dx \leq \liminf_{k \rightarrow \infty} \int_{\Omega} F(x, u_n(x)) dx.$$

Example 56 (Poisson equation). A solution of the Poisson equation with homogeneous Dirichlet boundary conditions

$$\begin{cases} \Delta u = f & \Omega, f \in L^2(\Omega) \\ u = 0 & \partial\Omega, \end{cases}$$

is a minimum of the following functional defined on $H_0^1(\Omega) = \overline{\mathcal{D}(\Omega)}^{H^1(\Omega)}$

$$F(u) = \frac{1}{2} \int_{\Omega} |\nabla u|^2 dx - \int_{\Omega} fu dx.$$

First, this functional admits a minimum. Indeed, $|\nabla u|^2 - fu$ is convex, so that $F(u)$ is a convex functional. Moreover if $u_n \xrightarrow{H^1(\Omega)} u$, then $\|\nabla u_n\|_{L^2(\Omega)}^2 \rightarrow \|\nabla u\|_{L^2(\Omega)}^2$,

so that

$$\begin{aligned} |F(u_n) - F(u)| &\leq \frac{1}{2} \left| \|\nabla u_n\|_{L^2(\Omega)}^2 - \|\nabla u\|_{L^2(\Omega)}^2 \right| + \int_{\Omega} |f(u_n - u)| dx \\ &\leq \frac{1}{2} \left| \|\nabla u_n\|_{L^2(\Omega)}^2 - \|\nabla u\|_{L^2(\Omega)}^2 \right| + \|f\|_{L^2(\Omega)} \|u_n - u\|_{L^2(\Omega)} \xrightarrow{n \rightarrow \infty} 0. \end{aligned}$$

The last inequality comes from Hölder inequality. Hence the functional F is continuous, therefore l.s.c. To prove that the functional is coercive, recall that

$$F(u) = \|\nabla u\|_{L^2(\Omega)}^2 - \int_{\Omega} f u dx.$$

It will be necessary to use Poincaré inequality to get

$$\|\nabla u\|_{L^2(\Omega)} \geq C \|u\|_{H_0^1(\Omega)}$$

Hence the term $\|\nabla u\|_{L^2(\Omega)}^2$ is more than quadratic in $\|u\|_{H_0^1(\Omega)}$. On the other side, by Hölder,

$$\left| \int_{\Omega} f u dx \right| \leq \tilde{C} \|u\|_{L^2(\Omega)} \leq \tilde{C} \|u\|_{H_0^1(\Omega)},$$

which gives that the second term is less than linear in $\|u\|_{H_0^1(\Omega)}$. Therefore

$$\lim_{\|u\|_{H_0^1(\Omega)} \rightarrow \infty} F(u) = \infty.$$

So that F is continuous convex and coercive. Since $H_0^1(\Omega)$ is reflexive, theorem 54 ensures that F admits a minimum.

To actually find the minimum, we first find the Euler-Lagrange equation of F by computing directional derivatives of F . If u is a minimum, all the directionnal

derivatives should vanish. Let $v \in \mathcal{D}(\Omega)$, then

$$\begin{aligned}
\frac{\partial F}{\partial v}(u) &= \left. \frac{d}{dt} F(u + tv) \right|_{t=0} \\
&= \left. \frac{d}{dt} \frac{1}{2} \int_{\Omega} |\nabla u + t\nabla v|^2 dx + \int_{\Omega} f(u + tv) dx \right|_{t=0} \\
&= \frac{1}{2} \int_{\Omega} \left. \frac{d}{dt} |\nabla u + t\nabla v|^2 \right|_{t=0} dx + \int_{\Omega} \left. \frac{d}{dt} f(u + tv) \right|_{t=0} dx \\
&= \int_{\Omega} (\nabla u + t\nabla v) \cdot \nabla v \Big|_{t=0} dx + \int_{\Omega} f'v \Big|_{t=0} dx \\
&= \int_{\Omega} \nabla u \cdot \nabla v dx + \int_{\Omega} f v dx \\
&= (\nabla u, \nabla v)_{\mathcal{D}(\Omega)} (f, v)_{\mathcal{D}(\Omega)} \\
&= (-\Delta u, v)_{\mathcal{D}(\Omega)} + (f, v)_{\mathcal{D}(\Omega)} \\
&= (-\Delta u + f, v)_{\mathcal{D}(\Omega)} \\
&= 0, \quad \forall v \in \mathcal{D}(\Omega).
\end{aligned}$$

Hence $\Delta u = f$ in the sense of distributions. The solutions of that equation correspond to critical points of the functional. In order to solve numerically, it is possible to do a gradient descent which amounts to solve the initial value problem

$$\begin{cases} u_t = -\Delta u + f \\ u(x, 0) = g, \end{cases}$$

where g is some initial guess.

Chapter 3

IMAGE DENOISING

An image is seen as a function

$$g : \Omega \longrightarrow [0, 1]$$

representing the grey tones (0 for black and 1 for white). The domain Ω is in general a rectangle or a cube. The domain is bounded and there is a finite number of pixels in the image, hence it is natural to assume that $\|g\|_\infty < \infty$. The main goal of this work is to extract the heart geometry from the medical image g . Such images usually contain a lot of noise, coming from actual measurements imprecisions and errors in the image reconstruction process. Hence, the work has two parts:

- (1) Image denoising,
- (2) Segmentation.

But it turns out that both problems may be solved using similar techniques.

Denoising is a complex task that is very image dependant. Many types of noise can be found in images and they require different methods of denoising. The typical noise found in CT or MRI images is that some pixels, or small packets of pixels, will have a value slightly off the real value it should have. These errors can be big enough to lead to irrelevant segmentation. To repair these pixels, a common strategy is to apply a smoothing algorithm to the noisy image.

We present here several denoising techniques that admit PDE formulations, since they seem well adapted to our images and it turns out that the PDE's involved are very close to the ones that appears in the segmentation process.

There are several good references on the subject, let us only mention the book by Chan and Shen ([8]) and the one by Aubert and Kornprobst ([2]).

3.1. HEAT EQUATION

The most well known smoothing PDE is certainly the heat equation:

$$(\mathbf{P1}) \quad \begin{cases} u_t = \mu \Delta u, & \Omega \\ \frac{\partial u}{\partial n} = 0, & \partial\Omega \\ u_0 = g. \end{cases}$$

The physical interpretation of this equation is that Ω can be seen as a body with conductivity μ and that has a heat distribution given by g at time 0. The solution $u(x, t)$ represents the heat at pixel x at time t . The heat diffuses in the body and smooths pixels that are different from their neighbours. To solve the equation, it is necessary to specify a boundary condition. A common choice is to impose $\frac{\partial u}{\partial n} = 0$ on $\partial\Omega$, which means that no heat leaves the domain.

It is easy to solve $(\mathbf{P1})$ by finite differences when the domain has a rectangular shape. The domain is naturally discretized at each pixel. Let $u_{i,j}^n$ denote the value of the approach solution \bar{u} at pixel $x_{i,j}$ at time $n\Delta t$. As the spacing between pixel is constant here, we can take $\Delta x = \Delta y = 1$. Then

$$(u_t)_{i,j}^n \approx \frac{u_{i,j}^{n+1} - u_{i,j}^n}{\Delta t}.$$

The Laplacian discretized by central differences gives

$$(\Delta u)^n = u_{i+1,j}^n + u_{i-1,j}^n + u_{i,j+1}^n + u_{i,j-1}^n - 4u_{i,j}^n.$$

To solve the equation, it is necessary to choose at what time the Laplacian is to be evaluated. There are 3 main schemes:

- (1) $\Delta u \approx (\Delta u)^n$ (explicit)
- (2) $\Delta u \approx (\Delta u)^{n+1}$ (implicit)
- (3) $\Delta u \approx \frac{(\Delta u)^n + (\Delta u)^{n+1}}{2}$ (Crank-Nicholson)

The first scheme is called explicit since it is possible to solve u^{n+1} explicitly in term of u^n from the discretized equation

$$u_{i,j}^{n+1} = u_{i,j}^n + \mu\Delta t(u_{i+1,j}^n + u_{i-1,j}^n + u_{i,j+1}^n + u_{i,j-1}^n - 4u_{i,j}^n).$$

The other schemes need the resolution of a linear system of the form

$$Bu^{n+1} = Au^n \quad \Rightarrow \quad u^{n+1} = B^{-1}Au^n,$$

provided B is invertible. These schemes are less sensitive to instability, however, due to the size of the 3D medical images (about 50 000 000 voxels), it would be a huge challenge to solve such linear systems.

The desired image is the solution $u(x, \tau)$ for some time τ not too large. At steady state ($u_t = 0$), we have $u_{i,j}^n = u_{i,j}^{n+1} = u_{i,j}$, thus $\Delta u = 0$ leads to

$$u_{i,j} = \frac{u_{i+1,j} + u_{i-1,j} + u_{i,j+1} + u_{i,j-1}}{4}.$$

This means that the value at a pixel is the mean of the values of the neighbouring pixels. This is a discrete version of the property of harmonic functions which says that

$$\oint_{B_r(x)} u(y)dy = u(x)$$

for any ball $B_r(x) \subseteq \Omega$ about x .

One of the problem of that method is that it has the tendency to smooth edges. An other important issue is to determine the stopping time τ that gives the best smoothed image. That will be discussed later on. Changing the conductivity will make the solution to converge to steady state in less time, but the explicit scheme will need smaller time steps to remain stable, giving the same computation time.

Figure 3.1 shows results of smoothing via the heat equation.

on edges. The heat equation in divergence form is

$$(\mathbf{P2}) \quad \begin{cases} u_t = \operatorname{div}(\mu \nabla u), & \Omega \\ \frac{\partial u}{\partial n} = 0, & \partial\Omega \\ u_0 = g \end{cases}$$

where now μ is some function. Perona and Malik ([18]) initially proposed

$$\mu = e^{-\frac{|\nabla u|^2}{\sigma^2}}$$

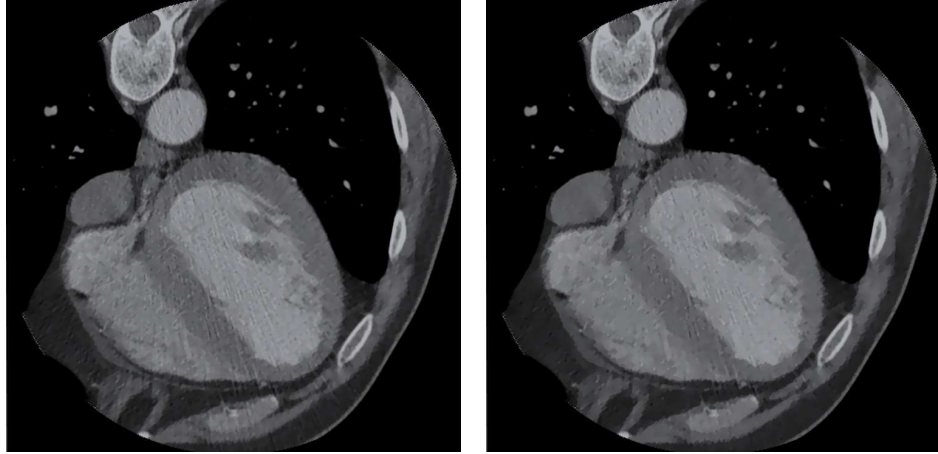
for some constant σ that depends on the actual image. A finite difference discretization of **(P2)** gives

$$\begin{aligned} u_{i,j}^{n+1} = & u_{i,j}^n + \Delta t (c_{i+1,j}^n (u_{i+1,j}^n - u_{i,j}^n) - c_{i-1,j}^n (u_{i,j}^n - u_{i-1,j}^n) \\ & + c_{i,j+1}^n (u_{i,j+1}^n - u_{i,j}^n) - c_{i,j-1}^n (u_{i,j}^n - u_{i,j-1}^n)). \end{aligned}$$

At steady states, this gives

$$u_{i,j} = \frac{c_{i+1,j} u_{i+1,j} + c_{i-1,j} u_{i-1,j} + c_{i,j+1} u_{i,j+1} + c_{i,j-1} u_{i,j-1}}{c_{i+1,j} + c_{i-1,j} + c_{i,j+1} + c_{i,j-1}},$$

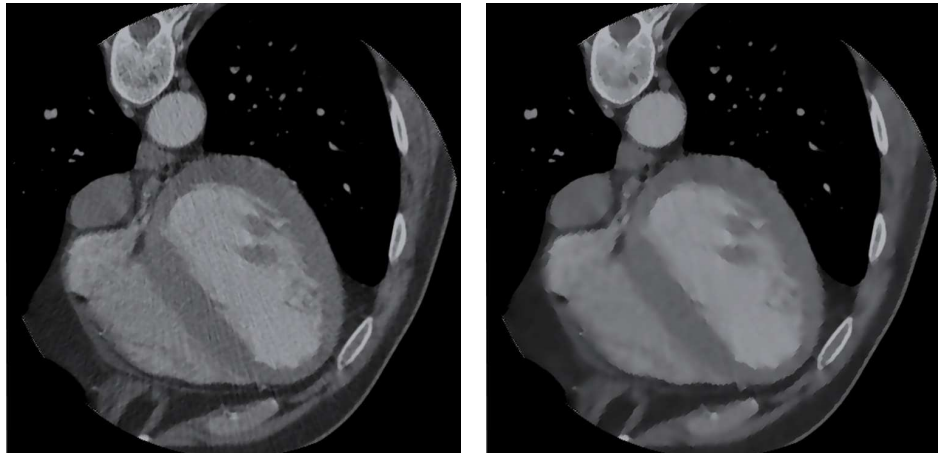
that is each pixel becomes a weighted average of its neighbours. The diffusion is anisotropic. If there is a jump between the pixels $x_{i,j}$ and $x_{i+1,j}$, then $c_{i+1,j}$ will be small and $u_{i,j}$ will depend mostly on other pixels. It is possible that the steady state is a good smoothing. In practice, this will have the tendency to smooth too much, except edges that are very clear. Figures 3.2 and 3.3 show results of anisotropic diffusion with $\sigma = 10$ and $\sigma = 20$. Figure 3.4 shows the steady state when $\sigma = 20$.



100 iterations

200 iterations

FIG. 3.2. Smoothing via anisotropic diffusion with $\Delta t = 0.1$ and $\sigma = 10$. The parameter σ is slightly too small, some noise is kept while the rest gets smoother.



50 iterations

200 iterations

FIG. 3.3. Smoothing via anisotropic diffusion with $\Delta t = 0.1$ and $\sigma = 20$. Now, noise is removed, but some edges tend to disappear as the one between the cavity of the heart and the muscle.



FIG. 3.4. The steady state when $\sigma = 20$. Most details have disappeared.

3.3. SOBOLEV SMOOTHING

In this section, we start to investigate variational formulations of the denoising problem. The idea behind this is that the ideal image will minimize a certain functional.

$$E : V \longrightarrow \mathbb{R},$$

where V is the vector space of admissible images, that has to be well chosen in order for E to admit a minimum. The choice of functional will be very image dependant.

Example 57 (Sobolev smoothing).

$$E : H^1(\Omega) \longrightarrow \mathbb{R},$$

$$u \mapsto \int_{\Omega} |\nabla u|^2 dx + \int_{\Omega} (u - g)^2 dx.$$

The functional is coercive, convex and continuous (hence l.s.c.) on $W^{1,2}(\Omega)$. Therefore E reaches its minimum at some $u \in W^{1,2}(\Omega)$. We compute the directional derivatives of E at u :

$$\begin{aligned}
\frac{\partial E}{\partial v}(u) &= \left. \frac{d}{dt} E(u + tv) \right|_{t=0} \\
&= \left. \frac{d}{dt} \int_{\Omega} |\nabla u + t\nabla v|^2 dx + \int_{\Omega} (u + tv - g)^2 dx \right|_{t=0} \\
&= \int_{\Omega} \left. \frac{d}{dt} |\nabla u + t\nabla v|^2 \right|_{t=0} dx + \int_{\Omega} \left. \frac{d}{dt} (u + tv - g)^2 \right|_{t=0} dx \\
&= 2 \int_{\Omega} (\nabla u + t\nabla v) \cdot \nabla v \Big|_{t=0} dx + 2 \int_{\Omega} (u + tv - g)v \Big|_{t=0} dx \\
&= 2 \left[\int_{\Omega} \nabla u \cdot \nabla v dx + \int_{\Omega} (u - g)v dx \right] \\
&= 2 [(\nabla u, \nabla v)_{\mathcal{D}(\Omega)} + (u - g, v)_{\mathcal{D}(\Omega)}] \\
&= 2 [-(\Delta u, v)_{\mathcal{D}(\Omega)} + (u - g, v)_{\mathcal{D}(\Omega)}] \\
&= 2(-\Delta u + (u - g), v)_{\mathcal{D}(\Omega)} \\
&= 0, \quad \forall v \in \mathcal{D}(\Omega).
\end{aligned}$$

Hence

$$\Delta u = u - g$$

in the sense of distributions, which is the Euler-Lagrange equation of E . The equation associated to the gradient descent is

$$(\mathbf{P3}) \begin{cases} u_t = \Delta u + (g - u), & \Omega \\ \frac{\partial u}{\partial n} = 0, & \partial\Omega \\ u(x, 0) = g. \end{cases}$$

In principle, the initial condition could be any function, but it is reasonable to take g as initial guess. The steady state of that equation will be a solution of $\Delta u = u - g$ that correspond to a local minimum of the functional. This is the desired image.

However, in this ideal image, sharp edges have disappeared. For example, let $\Omega = \mathbb{R}$ and $g = \chi_{(0,1)}$. g is an ideal image that do not need to be cleaned. To estimate $\int_{\Omega} |\nabla g|^2 dx$, approach g by functions f_n (See figure 3.5). :

$$f_n = \begin{cases} nx + 1, & x \in [-1/n, 0) \\ 1, & x \in [0, 1] \\ -nx + n + 1, & x \in (1, 1 + 1/n] \\ 0, & \text{else.} \end{cases}$$

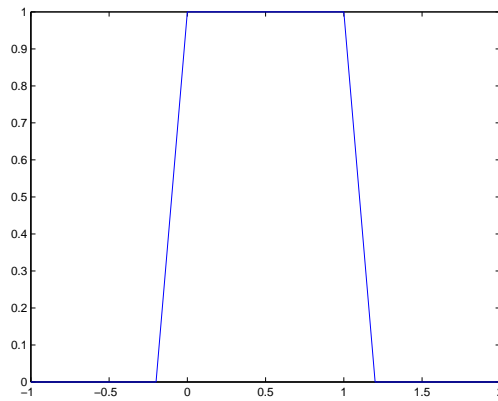


FIG. 3.5. The function f_5

Now, compute

$$\int_{\Omega} |\nabla f_n|^2 = 2n^2 \frac{1}{n} = 2n \xrightarrow{n \rightarrow \infty} \infty,$$

which yields $E(f_n) \rightarrow \infty$. Hence the minimum of E will be far from g .

This calculation suggest that it would be more natural to consider the L^1 -norm of the derivative instead of the L^2 -norm. This leads to Total Variation functional.

3.4. TOTAL VARIATION

Introduced by Osher, Fatemi and Rudin[19], the idea is to minimize the functional

$$E : BV(\Omega) \longrightarrow \mathbb{R},$$

$$u \mapsto \mu |Du|(\Omega) + \int_{\Omega} (u - g)^2 dx.$$

Note that if $u \in W^{1,1}(\Omega)$, then

$$|Du|(\Omega) = \int_{\Omega} d|Du| = \int_{\Omega} |\nabla u| dx.$$

An obvious advantage is that discontinuous functions are admissible as long as their approximate discontinuity set is of finite \mathcal{H}^{N-1} measure. In the last example, the image $g = \chi_{(0,1)}$ is certainly a minimum of E .

Let's compute the Euler-Lagrange equation of E . Let $v \in \mathcal{D}(\Omega)$, then formally

$$\begin{aligned} \frac{\partial E}{\partial v} &= \mu \frac{d}{dt} |Du + t\nabla v|(\Omega) \Big|_{t=0} + 2(u - g) \\ &= \left(\mu \frac{Du + t\nabla v}{|Du + t\nabla v|} \cdot \nabla v \right) (\Omega) \Big|_{t=0} + 2(u - g) \\ &= \left(\mu \frac{Du}{|Du|} \cdot \nabla v \right) (\Omega) \Big|_{t=0} + 2(u - g) \\ &= \left(\mu \frac{Du}{|Du|}, \nabla v \right)_{\mathcal{D}(\Omega)} + 2(u - g) \\ &= \left(-\mu \operatorname{div} \left(\frac{Du}{|Du|} \right), v \right)_{\mathcal{D}(\Omega)} + 2(u - g) \\ &= \left(-\mu \operatorname{div} \left(\frac{Du}{|Du|} \right) + 2(u - g), v \right)_{\mathcal{D}(\Omega)} \\ &= 0, \quad \forall v \in \mathcal{D}(\Omega). \end{aligned}$$

Hence

$$\mu \operatorname{div} \left(\frac{\nabla u}{|\nabla u|} \right) = u - g$$

in the sense of distributions, which is the Euler-Lagrange equation of E . The equation associated to the gradient descent is

$$(\mathbf{P4}) \begin{cases} u_t = \mu \operatorname{div} \left(\frac{\nabla u}{|\nabla u|} \right) + (g - u), & \Omega \\ \frac{\partial u}{\partial n} = 0, & \partial\Omega \\ u(x, 0) = g. \end{cases}$$

Again, the initial condition could be any function, but it is reasonable to take g as initial guess. The steady state of that equation will be the desired image. Note that for a function $u : \Omega \rightarrow \mathbb{R}$, $\frac{\nabla u}{|\nabla u|}$ is a unit normal vector to the level curves and then $\operatorname{div} \left(\frac{\nabla u}{|\nabla u|} \right)$ is simply the mean curvature of the level curves. Therefore the Total Variation algorithm will smooth the level curves of the initial image g . The greater μ is, the more regular the steady state will be.

The Euler-Lagrange equation is non-linear and exhibits unstable numerical behaviour, which force us to take very small time steps. Especially, when an explicit time scheme is used. An implicit scheme would be better, but we would have to use Newton's method to solve at each time step, which requires solving several linear systems and that is too demanding for large 3D images. Moreover, an explicit solver is easily parallelizable.

Another challenging part is to discretize the curvature term $\operatorname{div} \left(\frac{\nabla u}{|\nabla u|} \right)$. This term is highly non linear and behaves badly when u is nearly flat. There are several ways to discretize this term. A first approach is to compute

$$\begin{aligned} \operatorname{div} \left(\frac{\nabla u}{|\nabla u|} \right) &= \frac{\partial}{\partial x} \left(\frac{u_x}{\sqrt{u_x^2 + u_y^2}} \right) + \frac{\partial}{\partial y} \left(\frac{u_y}{\sqrt{u_x^2 + u_y^2}} \right) \\ &= \dots = \frac{u_y^2 u_{xx} - 2u_x u_y u_{xy} + u_x^2 u_{yy}}{(u_x^2 + u_y^2)^{3/2}}. \end{aligned}$$

Then each of u_x , u_y , u_{xx} , u_{yy} , u_{xy} can be discretized by centered differences. It is a natural choice to use central differences since $\operatorname{div} \left(\frac{\nabla u}{|\nabla u|} \right)$ is a diffusive term, there is no preferred direction.

Recall that the curvature of a curve at a point x is $1/r$, where r is largest radius of a tangent circle to the curve at x . Then it seems natural to impose that

$$\left| \operatorname{div} \left(\frac{\nabla u}{|\nabla u|} \right) \right|_{i,j} < \frac{1}{\Delta x},$$

since we cannot hope to resolve curvature in the image at points where the given radius is smaller than the size of a pixel. It turns out that imposing this condition stabilizes the scheme.

An other approach is to discretize directly

$$\begin{aligned} \frac{\partial}{\partial x} \left(\frac{u_x}{\sqrt{u_x^2 + u_y^2}} \right) (x_{i,j}) &\approx \frac{\frac{(u_{i+1,j} - u_{i,j})}{h}}{\sqrt{\frac{(u_{i+1,j} - u_{i,j})^2}{h^2} + \frac{(u_{i,j+1} - u_{i,j-1})^2}{4h^2} + \delta}} \\ &\quad - \frac{\frac{(u_{i,j} - u_{i-1,j})}{h}}{\sqrt{\frac{(u_{i,j} - u_{i-1,j})^2}{h^2} + \frac{(u_{i-1,j+1} - u_{i-1,j-1})^2}{4h^2} + \delta}}, \end{aligned}$$

where δ is some small parameter (typically $\delta = 10^{-10}$) that avoids divisions by zero. With the introduction of this parameter, it is not necessary to test whether $\left| \operatorname{div} \left(\frac{\nabla u}{|\nabla u|} \right) \right|_{i,j} < \frac{1}{\Delta x}$ or not.

The partial derivatives are discretized sometimes via forward, sometimes via centered differences. This choice may seem strange, but a completely centered scheme would involve values that are two pixels away from the center $x_{i,j}$, which is a too wide window. Moreover, it is computationally more expensive to check boundary conditions in this case.

To avoid the use of a non centered scheme, it is possible to introduce middle points $x_{i\pm 1/2,j}$ and $x_{i,j\pm 1/2}$, together with values

$$u_{i\pm 1/2,j} = \frac{u_{i,j} + u_{i\pm 1,j}}{2} \quad \text{and} \quad u_{i,j\pm 1/2} = \frac{u_{i,j} + u_{i,j\pm 1}}{2}.$$

Then a centered scheme would be

$$\frac{\partial}{\partial x} \left(\frac{u_x}{\sqrt{u_x^2 + u_y^2}} \right) (x_{i,j}) \approx \frac{\frac{(u_{i+1,j} - u_{i,j})}{h}}{\sqrt{\frac{(u_{i+1,j} - u_{i,j})^2}{h^2} + \frac{(u_{i+1/2,j+1} - u_{i+1/2,j-1})^2}{4h^2}}} + \delta$$

$$- \frac{\frac{(u_{i,j} - u_{i-1,j})}{h}}{\sqrt{\frac{(u_{i,j} - u_{i-1,j})^2}{h^2} + \frac{(u_{i-1/2,j+1} - u_{i-1/2,j-1})^2}{4h^2}}} + \delta$$

We couldn't determine experimentally if one of these schemes is better than the others. The performance of each of these is really image dependant. However, if we discretize the equation

$$u_t = \operatorname{div} \left(\frac{\nabla u}{|\nabla u|} \right)$$

with the second scheme and a forward Euler scheme in time, we get

$$u_{i,j}^{n+1} = u_{i,j}^n + \Delta t (\mu (C_{i,j} u_{i+1,j}^n + C_{i-1,j} u_{i,j}^n + D_{i,j} u_{i,j+1}^n + D_{i,j-1} u_{i,j-1}^n) \quad (3.4.1)$$

$$- (C_{i,j} + C_{i-1,j} + D_{i,j} + D_{i,j-1}) u_{i,j}^n), \quad (3.4.2)$$

where

$$C_{i,j}^n = \frac{1}{\sqrt{\frac{(u_{i+1,j}^n - u_{i,j}^n)^2}{h^2} + \frac{(u_{i,j+1}^n - u_{i,j-1}^n)^2}{4h^2}}}$$

and similarly

$$D_{i,j}^n = \frac{1}{\sqrt{\frac{(u_{i,j+1}^n - u_{i,j}^n)^2}{h^2} + \frac{(u_{i+1,j}^n - u_{i-1,j}^n)^2}{4h^2}}}$$

Chan and Vese [24] suggested that replacing $\phi_{i,j}^n$ by $\phi_{i,j}^{n+1}$ in the right hand side of 3.4.1 improves the stability of the algorithm. This can still be solved explicitly, indeed

$$u_{i,j}^{n+1} = \frac{1}{C} (u_{i,j}^n + \Delta t (\mu (C_{i,j} u_{i+1,j}^n + C_{i-1,j} u_{i,j}^n + D_{i,j} u_{i,j+1}^n + D_{i,j-1} u_{i,j-1}^n)),$$

where

$$C = 1 + \Delta t \mu (C_{i,j} + C_{i-1,j} + D_{i,j} + D_{i,j-1}).$$

They called this a semi-explicit scheme. Experimentally, this scheme has proven his superiority over the others, but to our knowledge, there is no rigorous justification of that fact. It will be the preferred scheme for discretizing curvature terms. Figure 3.6 shows the result of applying this equation for smoothing images.

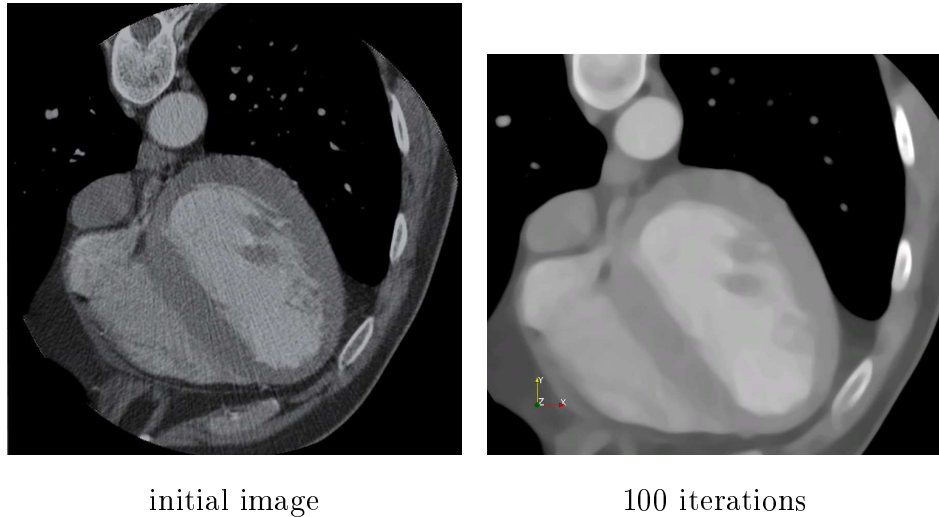


FIG. 3.6. Smoothing via total variation with $\mu = 100$

Remark 58. *The variational approach suggest a criterion for what would be a good stopping time when an image is smoothed via the heat equation or by anisotropic diffusion: one should stop when either the Sobolev energy, or the total variation energy is minimal. This correspond to minimizing the corresponding energy on a one dimensional family of images, namely the solution $u(x, t)$ of the problem (P1) or (P2).*

Total variation method is very efficient for wipe noise on relatively uniform objects. There is currently a lot of research that is done in order to improve this method. The main goal is to be able to use it on objects with texture, see for example [3] or [14].

Chapter 4

SEGMENTATION PROBLEM

Once the medical image is cleaned appropriately, it is possible to tackle the segmentation problem, that is to separate the image into its “significant” components. Here, the meaning of “significant” relies on the goal pursued by the segmenters. To segment the image, it is possible to look for regions or edges. Of course, one defines the other, but the underlying principles and techniques may be quite different.

4.1. ACTIVE CONTOURS (SNAKE)

We begin by describing the Active contour model introduced by Kass et al. [12]. In the active contours algorithm, we seek for the edges of an image. The set of admissible edges is the set V of closed continuous curves in Ω (often called *snakes*). For simplicity, we will assume that it has one connected component.

$$V = \{v : S^1 \longrightarrow \Omega\}.$$

To know which one approximates best the boundaries we define a curve energy. The energy of $v : S^1 \longrightarrow \Omega$ is defined as

$$E_{\text{snake}}(v) = E_{\text{int}}(v) + E_{\text{ext}}(v).$$

$E_{\text{int}}(v)$ is the internal energy, which decreases as v gets more regular. Typically

$$E_{\text{int}}(v) = \int_{S^1} \left| \frac{dv}{ds} \right|^2 ds + \alpha \int_{S^1} \left| \frac{d^2v}{ds^2} \right|^2 ds.$$

The first term is an elasticity term, that penalizes long curves. The second is a rigidity term, that penalizes high curvature regions.

The external energy $E_{\text{ext}}(v)$ must be related to the underlying image. It must be small if v is on the edges of g , which are characterized by pixels with large gradient. There are many possibilities for $E_{\text{ext}}(v)$. A common one is

$$E_{\text{ext}}(v) = -\beta \int_{S^1} |\nabla g(v(s))|^2 ds,$$

but it could be $-\int_{S^1} h(|\nabla g(v(s))|) ds$, for any increasing positive function h .

Remark 59. *The energy functional is non convex. It does have minimizers, but they need not be unique.*

It is then possible to compute the Euler-Lagrange equation of this minimization problem. The problem is usually solved by a gradient descent method, starting from an initial curve v_0 . In general, if the initial curve is close to the curve we seek, this approach will give interesting results, since the initial curve is close to the global minimum of the functional.

On the other end, when the initial curve is relatively far, many problems may appear. First, the curve can get stuck in a local minimum. An other problem is that we may want the curve to change topology or to avoid overcrossings. These operations are hard to do with a parametrized curve. The algorithm to evolve a parametrized curve usually goes as follows

- (1) Discretize the curve
- (2) Advance the front by an explicit or implicit scheme
- (3) Reparametrize the curve.

The reparametrization is very important since the curve may be stretched or compressed at some places. Figure 4.1 shows how this can be complicated when there is a possibility for a change of topology.

4.2. LEVEL SET METHOD

The *Level Set method* was introduced in the 90's by Sethian and Osher [17]. This method give tools to evolve a curve and manage topology changes, which

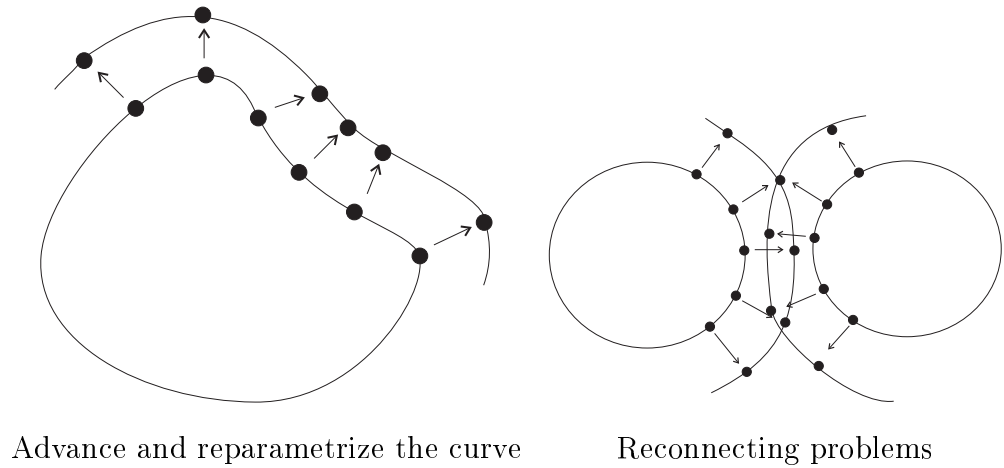


FIG. 4.1. Active contours with a parametrized curve

was hard with the classical Active Contours approach. The idea is simple: instead of describing the curve via an explicit parametrization $C = \{v(s), s \in S^1\}$, the curve is described implicitly via a function

$$\phi : \Omega \longrightarrow \mathbb{R},$$

such that

$$C = \{x : \phi(x) = 0\}.$$

The curve evolution can then be describe as a function

$$\phi : \Omega \times \mathbb{R}^+ \longrightarrow \mathbb{R},$$

such that the curve C_t at time t is simply

$$C_t = \{x : \phi(x, t) = 0\}.$$

Example 60 (Level set formulation of active contours of Kass et al.). *We can describe the curve in the active contour of Kass et al. [12] via a level set function*

$$\phi : \Omega \longrightarrow \mathbb{R}.$$

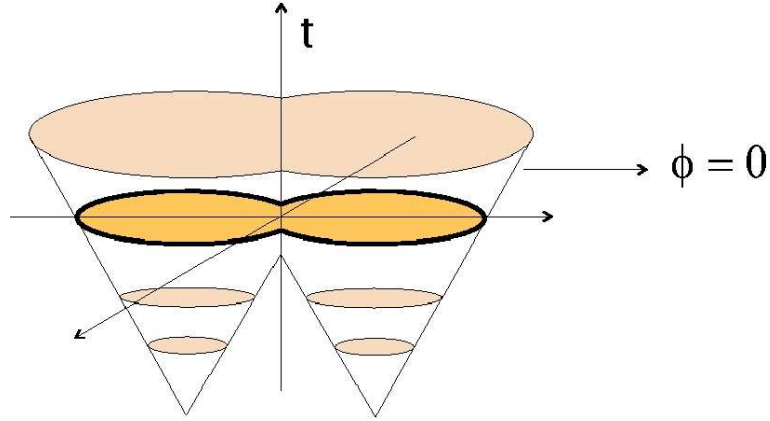


FIG. 4.2. The level set method can handle topology changes of the curve. Different slices, that correspond to different times in the curve evolution process are shown.

Then

$$E_{\text{int}}(v) = \mathcal{H}^{N-1}(\{\phi = 0\}) + \alpha \int_{\Omega} \delta(\phi) \operatorname{div} \left(\frac{\nabla \phi}{|\nabla \phi|} \right) dx$$

The first term in the energy computes the length and the second integrates the mean curvature of the curve (the 0 level curve of ϕ). Now remark that if $H = \chi_{[0, \infty)}$ denote the heavyside function

$$\mathcal{H}^{N-1}(\{\phi = 0\}) = |DH(\phi)|(\Omega) = \int_{\Omega} d|DH(\phi)| = \int_{\Omega} \delta(\phi) |\nabla \phi| dx.$$

Hence

$$E_{\text{int}}(v) = \int_{\Omega} \delta(\phi) |\nabla \phi| dx + \alpha \int_{\Omega} \delta(\phi) \operatorname{div} \left(\frac{\nabla \phi}{|\nabla \phi|} \right) dx$$

is the level set formulation of the internal energy. As it will be noted in section 4.5, the term associated to $\int_{\Omega} \delta(\phi) |\nabla \phi| dx$ in the Euler-Lagrange equation has the form

$$\delta(\phi) \operatorname{div} \left(\frac{\nabla \phi}{|\nabla \phi|} \right),$$

which accounts for the rigidity term. Hence minimizing length gives rise to a curvature term in the curve evolution process. This suggests some dependance between the two terms in the internal energy. It has been suggested to take only the first one [5].

Using the level set formulation, it is also possible to devise a curve evolution that does not necessarily come from a minimization problem. For example

$$(\mathbf{P5}) \begin{cases} \phi_t = -V_n |\nabla \phi| \\ \phi(x, 0) = \phi_0 \end{cases}$$

evolves the curve described by ϕ_0 in the normal direction at a speed V_n . Indeed, if $v(t)$ is a parametrisation of the curve at time t , then

$$0 = \frac{d}{dt} \phi(v(t), t) = \phi_t + \nabla \phi(v(t), t) \cdot v'(t).$$

But as noted before the normal to the curve is $n = \frac{\nabla \phi}{|\nabla \phi|}$ and since the normal speed is $v'(t) \cdot n = V_n$, we get

$$0 = \phi_t + \nabla \phi(v(t), t) \cdot v'(t) = \phi_t + |\nabla \phi| n \cdot v'(t) = \phi_t + V_n |\nabla \phi|.$$

The normal speed V_n can depend on various things such as

- (1) Position in space
- (2) External parameters (e.g. medical image g)
- (3) Curvature of the curve.

Example 61. Let $h : \mathbb{R}^+ \rightarrow \mathbb{R}^+$ be an edge stopping function, ie. such that

- (1) h is monotonely decreasing,
- (2) $h(0) = 1$,
- (3) $h(x) \xrightarrow{x \rightarrow \infty} 0$.

Now, consider the problem

$$\begin{cases} \phi_t = h(|\nabla g|) |\nabla \phi|, \\ \phi(\cdot, 0) = \phi_0. \end{cases}$$

This will evolve the initial curve $C_0 = \{\phi_0 = 0\}$, that moves in the normal direction with constant speed in objects with uniform colors, and stops when it reaches points of high gradient of g (a boundary point). It is possible to refine the model, by adding a curvature term

$$V_n = h(|\nabla g|) + \epsilon \kappa.$$

This will prevent the curve to form sharp corners. This process is local: it may get stucked into closed regions. In such a case, it may not detect features over these boundaries.

There are now many books available on that method, since it revealed itself as a very efficient and robust way to model the evolution of curves and fronts. The main ones are the book by Sethian [22] and the one by Osher [19].

One of the main advantages of this method is that it handles topology changes. However, it may happen that in some circumstance, we have to control the topology of the regions $\{\phi > 0\}$ and $\{\phi < 0\}$. [11] proposes a way of doing so. When a pixel changes sign, *ie.* changes region, we need to know if this changes the topology. A simple criterion for that comes from digital topology [13].

4.3. MUMFORD-SHAH FUNCTIONAL

Now, let's go back to a promising minimization problem. Mumford and Shah [16] proposed that minimizing the functional

$$J(K, u) = \int_{\Omega \setminus K} |\nabla u|^2 + \int_{\Omega} (u - g)^2 + \mathcal{H}^{N-1}(K \cap \Omega)$$

over all admissible pairs $(K, u) \in \mathcal{A}$, where

$$\mathcal{A} = \{(K, u) : K \subseteq \bar{\Omega} \text{ compact}, u \in W_{\text{loc}}^{1,2}(\Omega \setminus K)\},$$

should give a good segmentation of the image $g \in L^\infty(\Omega)$. To prove that this problem admits a solution is really non trivial.

Let's try to solve this problem by the direct method. Take a minimizing sequence (K_n, u_n) . We can suppose that $\|u_n\|_\infty$ is uniformly bounded, say by $\|g\|_\infty$, otherwise, we can just truncate the sequence. The first thing we have to do is to provide the space $X = \{K \subseteq \bar{\Omega}, K \text{ compact}\}$ a topology.

Definition 62. (1) For $K \subseteq \bar{\Omega}$, we define $K_\epsilon = \{x \in X : \text{dist}(x, K) \leq \epsilon\}$.

(2) The Hausdorff distance between two compacts K and K' is

$$\delta(K, K') = \inf\{\epsilon : K \subseteq K'_\epsilon \text{ and } K' \subseteq K_\epsilon\}.$$

Theorem 63 (Blashke). (X, δ) is a compact metric space.

Now, we have the tools to show that the minimizing sequence (K_n, u_n) admits a converging subsequence. Since any sequence in X is bounded (Ω is bounded), we can suppose that our sequence K_n converges to some K . Now we wonder if u_n is converging to some function $u \in W_{\text{loc}}^{1,2}(\Omega)$. Let $A \subseteq B \subseteq \Omega$, with A open, B closed such that $B \cap K = \emptyset$. Then clearly there exists N such that for $n \geq N$, $B \cap K_n = \emptyset$. Then for $n \geq N$, $u_n \in W^{1,2}(A)$. Now since $\|u_n\|_\infty$ is uniformly bounded, there exists a subsequence converging weakly to $u \in W^{1,2}(A)$. By a diagonal argument, ranging over open subsets A of Ω , we can conclude that there is a subsequence of u_n converging weakly to $u \in W_{\text{loc}}^{1,2}(\Omega)$ [1].

So the sequence (K_n, u_n) has a subsequence that is converging to some pair (K, u) . The problem is that we cannot show that this pair actually minimizes the functional, since the functional is not lower semi-continuous with respect to this convergence. This comes from the fact that the function

$$K \mapsto \mathcal{H}^{N-1}(K)$$

is not l.s.c. In fact, any K can be approximated in an obvious way by discrete sets, which have \mathcal{H}^{N-1} -measure 0.

To bypass this, we have to go through a weak formulation of the problem. We search for $u \in SBV(\Omega)$ that minimizes the functional

$$F(u) = \int_{\Omega} |\nabla u|^2 + \int_{\Omega} (u - g)^2 + \mathcal{H}^{N-1}(S_u),$$

where now ∇u is the approximate gradient of u , ie. $Du = \nabla u \mathcal{L}^n + D^j u$, and S_u is the set of approximate discontinuities of u .

Remark 64. *It is a fact that Cantor functions ($Du = D^c u$) are dense in $L^2(\Omega)$. Those functions have $S_u = \emptyset$ and have no derivatives almost everywhere. Therefore*

$$\inf_{u \in BV(\Omega)} F(u) = 0;$$

This suggests that we really need to minimize over $SBV(\Omega)$.

The following theorem is crucial (see [1] for details). It shows the equivalence of the two formulations.

Theorem 65.

$$\inf_{u \in SBV(\Omega)} F(u) = \inf_{(K,u) \in \mathcal{A}} J(K, u).$$

The next important step is to prove that the weak formulation admits a solution.

Theorem 66. *Let $g \in L^\infty(\Omega)$. Then there exists $u \in SBV(\Omega)$ such that*

$$F(u) = \inf_{v \in SBV(\Omega)} F(v).$$

PROOF. F is bounded from below. So take a minimizing sequence u_n for F . We can suppose without loss of generality that $\|u_n\|_\infty \leq \|g\|_\infty$, since otherwise the sequence of functions $u'_n = \min(\|g\|_\infty, u_n)$ is such that $F(u'_n) \leq F(u_n)$. Therefore u'_n is also a minimizing sequence and satisfies the given property.

Since u_n is a minimizing sequence for F , clearly

$$\sup_n \left\{ \int_\Omega |\nabla u_n|^2 dx + \mathcal{H}^{N-1}(S_{u_n}) \right\} \leq \infty.$$

Then, using theorem 42, there exists $u \in SBV(\Omega)$ and a subsequence u_{n_k} of u_n such that $u_{n_k} \xrightarrow{*} u$. Now the map $v \mapsto \int_\Omega (g - v)^2 dx$ is strongly l.s.c. in $L^1(\Omega)$ by theorem 55. This, together with the second part of the theorem 41 ensures that

$$F(u) \leq \liminf_k F(u_{n_k}).$$

Thus $u \in SBV(\Omega)$ is a minimizer of F . □

4.4. PIECEWISE CONSTANT MUMFORD-SHAH PROBLEM

In practice, it is often necessary to simplify the problem to be able to compute the minimum numerically. One way is to minimize the Mumford-Shah functional over piecewise constant functions in $SBV(\Omega)$. It will produce good segmentation results only if the image is close to be constant inside the objects

of interest. First, the concept of a piecewise constant function has to be defined carefully (see [1] for details).

Definition 67. A partition $\{E_k\}_{k \in \mathbb{N}}$ of Ω is a Cacciopoli partition of Ω if

$$\sum_k P(E_k, \Omega) < \infty,$$

where $P(E_k, \Omega)$ denotes the perimeter of E_k in Ω . The partition is said to be ordered if the sequence $(|E_k|)$ is decreasing.

Definition 68. A function $u : \Omega \rightarrow \mathbb{R}$ is said to be piecewise constant if there exists a Cacciopoli partition $\{E_k\}$ of Ω and a sequence $\{t_k\}$ of real numbers such that

$$u = \sum_k t_k \chi_{E_k}.$$

Let $PC(\Omega)$ the set of piecewise constant functions over Ω .

Remark 69. The numbers t_k need not be distinct. But, they can be made distinct by ordering the set of values $\{t_{n_1}, t_{n_2}, \dots\}$ of u and taking the Cacciopoli partition $\{F_l\}$ of Ω given by

$$F_l = u^{-1}(t_{n_l}).$$

We call the $\{F_l\}$ the level set Cacciopoli partition of Ω associated to u .

It is important to understand how the discontinuity set of a piecewise constant function u can be. It turns out that \mathcal{H}^{N-1} -almost everywhere, $S_u \subseteq \bigcup_i \partial E_k \cap \Omega$. Therefore

$$2\mathcal{H}^{N-1}(S_u) \leq \sum_k P(E_k, \Omega).$$

It is clear that the equality need not be attained when the values t_k are not distinct. It turns out that this is the only possibility.

Theorem 70. Let u be piecewise constant function with level set Cacciopoli partition $\{E_k\}$ of Ω . Then

$$2\mathcal{H}^{N-1}(S_u) = \sum_k P(E_k, \Omega).$$

Cacciopoli partitions have nice compactness properties.

Theorem 71. *Let $\{E_{k,n}\}_n$ be a sequence of Cacciopoli partitions of Ω such that*

$$\sup_n \sum_k P(E_{k,n}, \Omega) < \infty.$$

Then there exists a Cacciopoli partition $\{E_k\}$ of Ω and a subsequence n_l such that for all k

$$\chi_{E_{k,n_l}} \xrightarrow{L^1} \chi_{E_k}.$$

With that in mind, it is possible to prove the existence of a minimizer for the piecewise constant Mumford-Shah problem.

Theorem 72. *Let $g \in L^\infty(\Omega)$. Then there exists $u \in SBV(\Omega) \cap PC(\Omega)$ such that*

$$F(u) = \inf_{v \in SBV(\Omega) \cap PC(\Omega)} F(v).$$

4.5. ACTIVE CONTOUR WITHOUT EDGES

Introduced by Chan and Vese [6] in 2001, this approach provides a way to find numerical solutions, at low computational cost of a simplified Mumford-Shah model. The idea is to describe the discontinuity set J_u by a level set function ϕ ,

$$J_u = \{\phi = 0\}.$$

Now, they proposed two approaches, that are to minimize over

- (1) functions differentiable on $\{\phi \neq 0\}$
- (2) binary functions ($u : \Omega \rightarrow \{c_1, c_2\}$, for $c_1, c_2 \in \mathbb{R}$).

The last one is certainly simpler. To describe a binary function, it is needed ϕ , that specifies the interface and the two values of the function c_1 and c_2 . The Mumford-Shah functional then becomes

$$F(u) = \mathcal{H}^{N-1}(J_u) + \int_{\Omega} (g - c_1)^2 H(\phi) dx + \int_{\Omega} (g - c_2)^2 (1 - H(\phi)) dx,$$

where $H = \chi_{[0, \infty)}$ stands for the Heavyside function. Now provided $c_1 \neq c_2$, we have that $J_u = \{\phi = 0\}$. Also, remark that

$$DH(\phi) = \delta(\phi) |\nabla \phi|,$$

so that

$$\mathcal{H}^{N-1}(J_u) = |DH(\phi)|(\Omega) = \int_{\Omega} \delta(\phi) |\nabla \phi| dx.$$

Then

$$F(u) = G(\phi, c_1, c_2) = \int_{\Omega} \delta(\phi) |\nabla \phi| dx + \int_{\Omega} (g - c_1)^2 H(\phi) dx + \int_{\Omega} (g - c_2)^2 (1 - H(\phi)) dx.$$

It is now possible to compute the Euler-Lagrange equation associated to F . We can compute the partial derivatives with respect to c_1 , c_2 and ϕ and set them to 0. Let's first compute $\frac{\partial F}{\partial c_1}$.

$$\begin{aligned} \frac{\partial F}{\partial c_1} &= \frac{\partial}{\partial c_1} \int_{\Omega} (g - c_1)^2 H(\phi) dx \\ &= -2 \int_{\Omega} (g - c_1) H(\phi) dx = 0. \end{aligned}$$

Hence

$$c_1 = \frac{\int_{\Omega} g H(\phi) dx}{\int_{\Omega} H(\phi) dx} \quad \text{and similarly} \quad c_2 = \frac{\int_{\Omega} g (1 - H(\phi)) dx}{\int_{\Omega} 1 - H(\phi) dx}.$$

Now, let's compute the directional derivative of E at ϕ in the direction $\psi \in \mathcal{D}(\Omega)$.

$$\begin{aligned} & \left. \frac{d}{dt} \int_{\Omega} \delta(\phi + t\psi) |\nabla \phi + t\nabla \psi| dx \right|_{t=0} \\ &= \int_{\Omega} \delta'(\phi + t\psi) \psi |\nabla \phi + t\nabla \psi| + \delta(\phi + t\psi) \frac{\nabla \phi + t\nabla \psi}{|\nabla \phi + t\nabla \psi|} \cdot \nabla \psi dx \Big|_{t=0} \\ &= \int_{\Omega} \delta'(\phi) \psi |\nabla \phi| + \delta(\phi) \frac{\nabla \phi}{|\nabla \phi|} \cdot \nabla \psi dx \end{aligned}$$

Remark that

$$\operatorname{div} \left(\delta(\phi) \frac{\nabla \phi}{|\nabla \phi|} \psi \right) = \delta'(\phi) |\nabla \phi| \psi + \delta(\phi) \operatorname{div} \left(\frac{\nabla \phi}{|\nabla \phi|} \right) \psi + \delta(\phi) \frac{\nabla \phi}{|\nabla \phi|} \cdot \nabla \psi$$

in the sense of distributions, so that

$$\begin{aligned} & \int_{\Omega} \delta'(\phi) \psi |\nabla \phi| + \delta(\phi) \frac{\nabla \phi}{|\nabla \phi|} \cdot \nabla \psi \, dx \\ &= \int_{\Omega} \operatorname{div} \left(\psi \delta(\phi) \frac{\nabla \phi}{|\nabla \phi|} \right) - \int_{\Omega} \delta(\phi) \operatorname{div} \left(\frac{\nabla \phi}{|\nabla \phi|} \right) \psi. \end{aligned}$$

Moreover

$$\int_{\Omega} \operatorname{div} \left(\delta(\phi) \psi \frac{\nabla \phi}{|\nabla \phi|} \right) = \int_{\partial \Omega} \delta(\phi) \psi \frac{\nabla \phi}{|\nabla \phi|} \cdot n \, d\mathcal{H}^{N-1} = 0$$

if we impose $\frac{\partial \phi}{\partial n} = \nabla \phi \cdot n = 0$, which seems a reasonable boundary condition, since this forces the level curves to be transverse to the boundary $\partial \Omega$. Therefore

$$\frac{d}{dt} \int_{\Omega} \delta(\phi + t\psi) |\nabla \phi + t\nabla \psi| \, dx \Big|_{t=0} = - \int_{\Omega} \delta(\phi) \operatorname{div} \left(\frac{\nabla \phi}{|\nabla \phi|} \right) \psi.$$

For the second term, we have

$$\begin{aligned} & \frac{d}{dt} \int_{\Omega} (g - c_1)^2 H(\phi + t\psi) \, dx + \int_{\Omega} (g - c_2)^2 (1 - H(\phi + t\psi)) \, dx \Big|_{t=0} \\ &= \int_{\Omega} (g - c_1)^2 \delta(\phi) \psi - (g - c_2)^2 \delta(\phi) \psi \, dx \\ &= \int_{\Omega} \delta(\phi) \psi [(g - c_1)^2 - (g - c_2)^2] \, dx \end{aligned}$$

Therefore

$$\begin{aligned} \left(\frac{\partial F}{\partial \phi}, \psi \right) &= - \int_{\Omega} \delta(\phi) \operatorname{div} \left(\frac{\nabla \phi}{|\nabla \phi|} \right) \psi + \int_{\Omega} \delta(\phi) \psi [(g - c_1)^2 - (g - c_2)^2] \, dx \\ &= \left(\delta(\phi) \left[-\operatorname{div} \left(\frac{\nabla \phi}{|\nabla \phi|} \right) + (g - c_1)^2 - (g - c_2)^2 \right], \psi \right) \\ &= 0, \quad \forall \psi \in \mathcal{D}(\Omega). \end{aligned}$$

Which means that

$$\delta(\phi) \left[-\operatorname{div} \left(\frac{\nabla \phi}{|\nabla \phi|} \right) + (g - c_1)^2 - (g - c_2)^2 \right] = 0$$

in the sense of distributions. In gradient descent form, this gives the initial value problem

$$(\mathbf{P6}) \begin{cases} \phi_t = \delta(\phi) \left[\operatorname{div} \left(\frac{\nabla \phi}{|\nabla \phi|} \right) - (g - c_1)^2 + (g - c_2)^2 \right], & \Omega \\ \frac{\partial \phi}{\partial n} = 0, & \partial \Omega \\ \phi(\cdot, 0) = \phi_0, \end{cases}$$

that is tight to the conditions

$$c_1 = \frac{\int_{\Omega} g H(\phi) dx}{\int_{\Omega} H(\phi) dx} \quad \text{and} \quad c_2 = \frac{\int_{\Omega} g(1 - H(\phi)) dx}{\int_{\Omega} 1 - H(\phi) dx}.$$

This equation is very close to the one obtained from the Total Variation algorithm of Osher. The main difference is that in this one we evolve a curve while with Osher algorithm it is the initial image g that is evolved. Also, in the last equation, there's a coefficient $\delta(\phi)$ so that only the 0 level set of ϕ moves. In practice, we will use a regularization δ_{ϵ} of δ .

$$\delta_{\epsilon}(x) = \frac{1}{\pi} \frac{\epsilon}{\epsilon^2 + x^2}$$

seems a good choice in many cases.

The algorithm for computing the solution then goes as follows: At each time step

- (1) Compute c_1 and c_2 from ϕ^n
- (2) Compute ϕ^{n+1} from ϕ^n , c_1 and c_2 .

This algorithm separates the given image g in 2 distinct parts. In general, that might not be sufficient to segment the image. Chan and Vese [6] proposed to evolve several curves instead of only one. n curves will separate the domain Ω in 2^n distinct regions. Each of these curve is represented by a level set function ϕ_i .

They managed to get some interesting results using 2 curves by solving the problem implicitly.

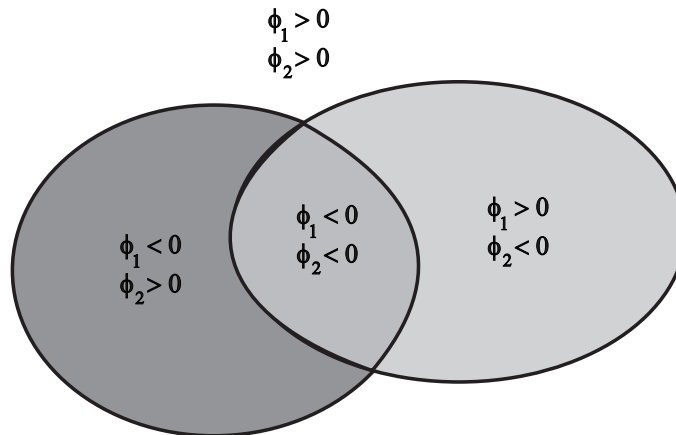


FIG. 4.3. The 4 regions determined by two level set functions ϕ_1 and ϕ_2 .

However, if we solve explicitly, the process become very unstable and as the 3D images are too big to solve implicitly, we proceeded in the following way. We first segment Ω with one curve, which separates Ω in 2 parts. Then we choose on of the two regions (for example the set $\{\phi > 0\}$), and segment it again, taking that region as the new domain Ω . This iterative segmentation process appears to work pretty well. An other alternative is to evolve a function that has more than 2 values. It has been proposed in [15].

As an initial image, it is a common choice to take the signed distance function to a given initial curve. That is $\phi_0(x) = \pm \text{dist}(x, C_0)$ with $\phi(x) > 0$ (resp. $\phi(x) < 0$) if x is in the exterior (resp. interior) of C_0 . The initial curve is often a circle, since the signed distance function is then easy to compute. However, it turns out that taking C_0 as a collection of equidistributed small circles accelerates the convergence (see figure 4.4). Also, this kind of initial curve allows us to use the same initial curve for each successive segmentations, since the curve will intersect almost each connected component of the new domain. Such a choice of initial condition is not necessary, but it speeds up the algorithm.

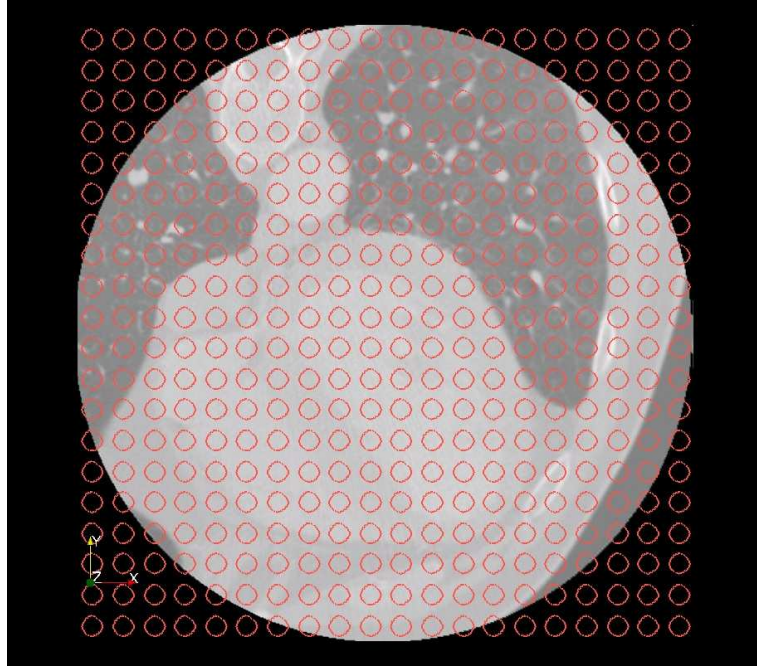


FIG. 4.4. An initial curve that has several connected components and that is equidistributed over the domain will help the algorithm to converge faster and it has more chances to actually find a global minimum.

Chan et al. [7] remarked that the algorithm often get stuck in local minimums. We also observed this problem, but we notice that it rarely happens when we take as initial curve a large set of small circles as described above. They recently proposed a way to bypass this problem. Basically, it is the term $\delta(\phi)$ in the equation that can block the evolution of the curve. They proposed to solve instead for

$$(\mathbf{P7}) \begin{cases} \phi_t = \operatorname{div} \left(\frac{\nabla \phi}{|\nabla \phi|} \right) - (g - c_1)^2 + (g - c_2)^2, & \Omega \\ \frac{\partial \phi}{\partial n} = 0, & \partial \Omega \\ \phi(\cdot, 0) = \phi_0. \end{cases}$$

A problem is that there will not be a steady state for that equation. The function ϕ will tend to ∞ outside the curve and to $-\infty$ inside. The idea is that for t large

enough, the level curve

$$C_r = \{\phi(\cdot, t) = r\}$$

will be a good contour for almost every choice of r .

Remark 73. *A signed distance function ϕ satisfies the equation*

$$|\nabla\phi| = 1$$

over Ω . Hence the level set equation becomes

$$\phi_t = \Delta\phi - (g - c_1)^2 + (g - c_2)^2,$$

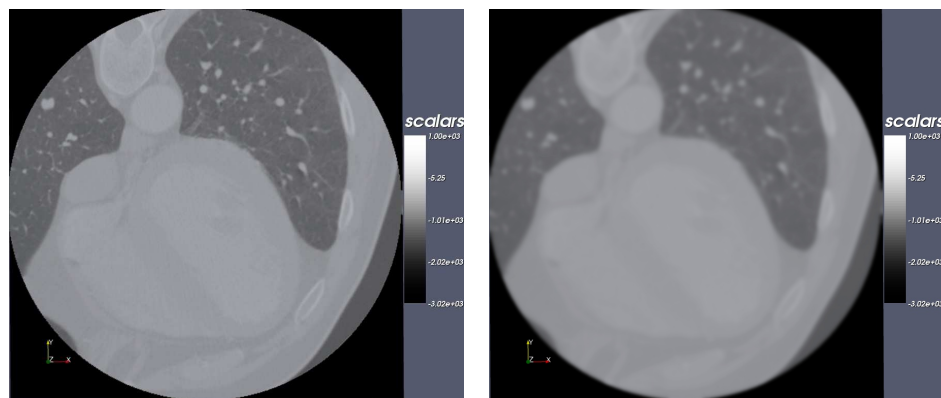
for which numerical schemes are less unstable than the scheme of the problems (P6) or (P7). The problem is that after a few time steps, the function ϕ may move far from a signed distance function. It is generally suggested to reinitialize ϕ to a signed distance function to its 0 level set frequently, to prevent it from distorting too much. However, we remarked that in our problem, instabilities (e.g. solution blows up) arise in the very first time steps, when ϕ is still very closed to a signed distance function. So we did not try to reinitialize the function.

4.6. NUMERICAL RESULTS

In this section, we show some numerical results obtained with the method of active contour without edges (problem (P6)) applied to a CT scan. We use iterative segmentations instead of evolving several curves at the same time since as we noted earlier, there is less stability problems, and the computational time is then dramatically decreased. The curvature term is discretized as described in section 3.4. As the spacing is constant, we set $\Delta x = \Delta y = 1$. For the regularization δ_ϵ of δ , we take $\epsilon = 1$ as suggested in [6]. At each time step, we compute the number of pixels that changed side of the curve. This gives an simple stopping criterion for the algorithm: stop when there is almost no pixels changing sign.

4.6.1. 2D results

We try to segment one slice shown in figure 4.5 (a) of a CT scan. It happens that to get a nice segmentation it is necessary at some stage of the segmentation to use a smoothed version of the given image. We simply applied the total variation algorithm for a small number of time steps.



(a) medical image

(b) smoothed version

FIG. 4.5. Initial images

The first two segmentation steps don't give any problem (see figure 4.6). The first step finds the external contour of the image (a circle), then we segment again the interior region of that circle (the red region in figure 4.6). These two segmentatoin are made with the original image.

For the next segmentation, it is necessary to use the smoothed image, otherwise, the noise influences too much the results, as can be seen in figure 4.7 (a). The same segmentation made with the smoothed image yields the result shown in figure 4.7 (b).

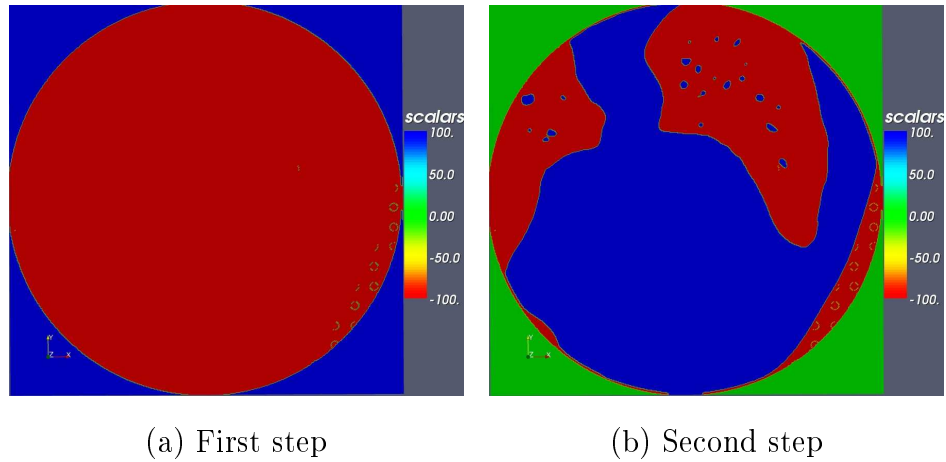


FIG. 4.6. First step finds the boundary of the image. The second isolates the lungs. The region in green has value 0. It is the region that has been rejected by the last step.

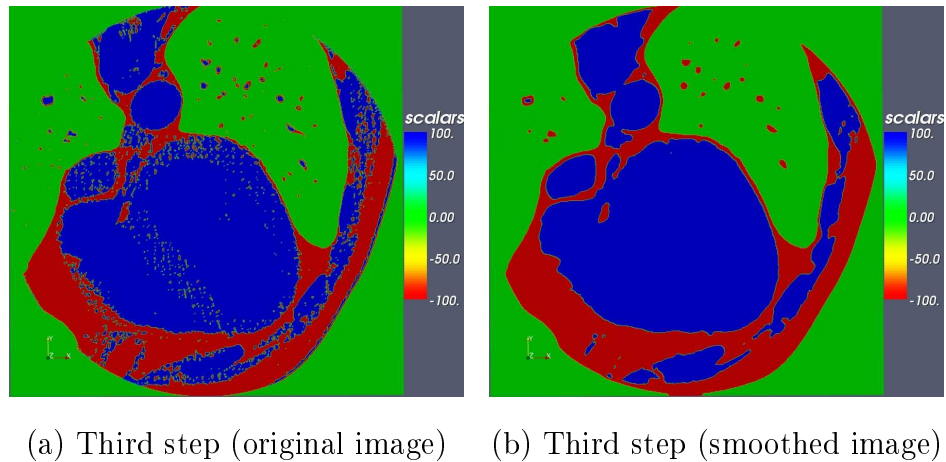


FIG. 4.7. Third step: it is necessary to smooth the image to have a good segmentation

Finally, a last segmentation step is performed to obtain the muscle of the heart. Figure 4.8 (a) shows the result of that segmentation and (b) is a clean version of (a), where only the heart is kept.

A summary of the different parameters and cpu time at different steps is shown in figure 4.6.1.

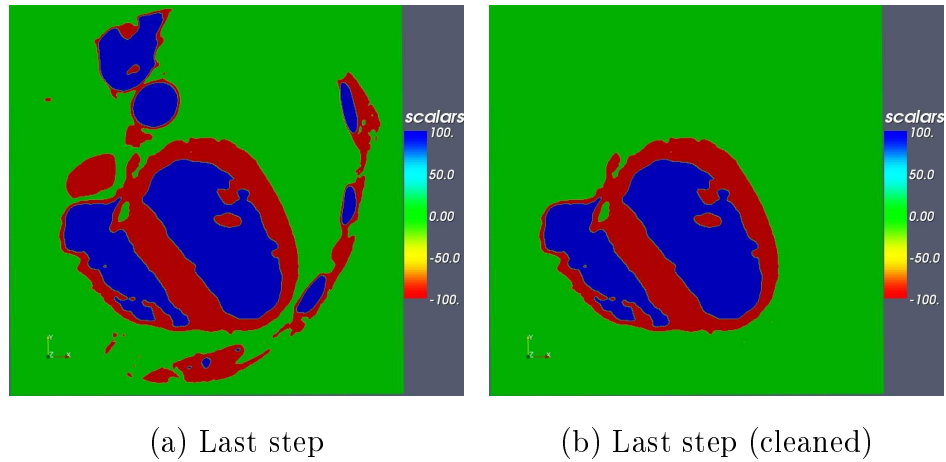


FIG. 4.8. The final result

Step	time step (Δt)	μ	Number of iterations	cpu time	cumulative cpu time
1	0.1	1	10	2.828s.	2.828s.
2	0.1	1	5	1.612s.	4.440s.
3	0.002	1	80	17.497s.	21.937s.
4	0.01	1	50	10.260s.	32.197s.

FIG. 4.9. Summary of 2D segmentation parameters

4.6.2. 3D results

We apply the same techniques to the 3D CT scan. Figures 4.10 to 4.12 show the several steps.

The 3D segmentation is not fully completed at the stage shown in figure 4.12. There remains parts that do not belong to the heart but that the level set function cannot separate.

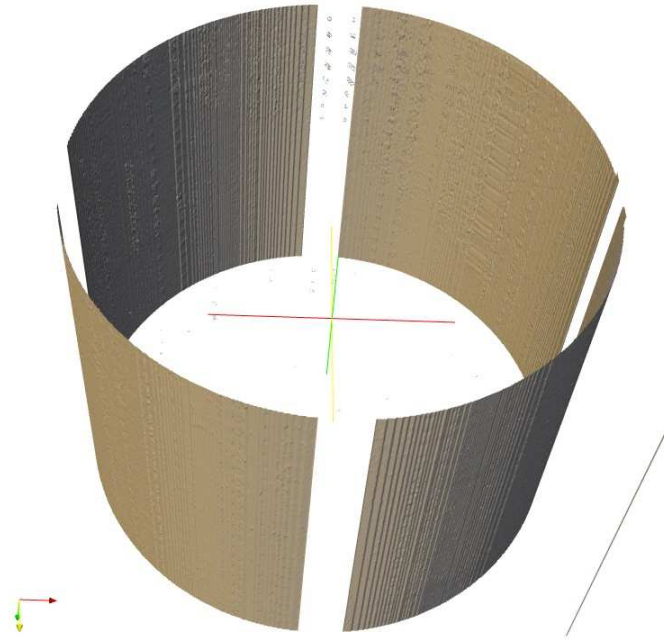


FIG. 4.10. First step: the cylinder boundary of the image is found.
We will next segment its interior

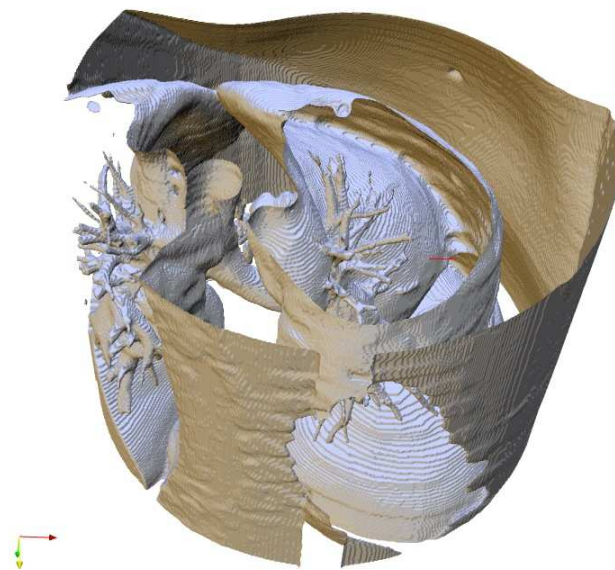


FIG. 4.11. Second step: the lunges are now segmented

A summary of the different parameters and cpu time at different steps is shown in figure 4.6.2.

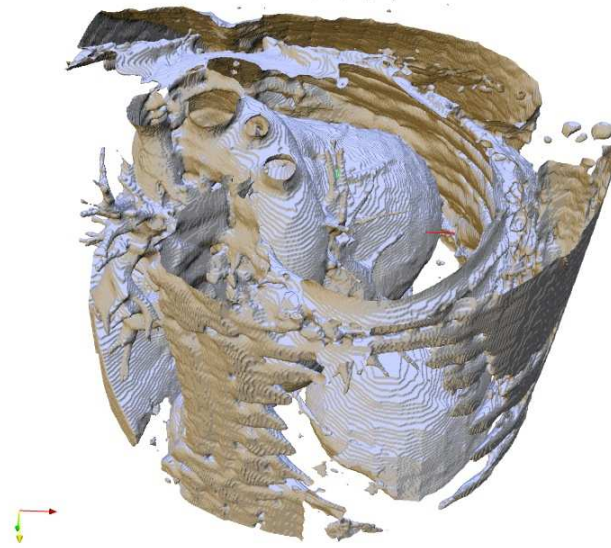


FIG. 4.12. Final step: the muscle of the heart is segmented.

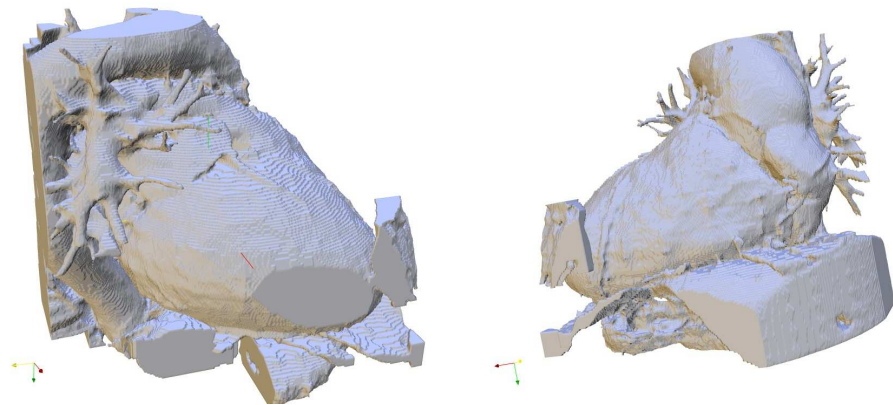


FIG. 4.13. Two views of the segmented heart

4.6.3. Computational remarks

In order to read and treat various formats of medical images, we use the C++ libraries named ITK. They have been developed by Kitware, under the cover of the National Library of Medicine and was designed to visualize and process images

Step	time step (Δt)	μ	Number of iterations	cpu time	cumulative cpu time
1	0.1	1	10	50s.	50s.
2	0.1	1	50	209s.	259s.
3	0.1	1	13	52s.	311s.
4	0.1	1	200	703s.	1014s.=16m54s.

FIG. 4.14. Summary of 3D segmentation parameters. For each computation, there is a reading and writing time of approximately 50s. This time is not included in the cpu time above.

from the Visible Human Project. It has nice and compact formats for images. Many algorithms are already implemented within ITK and they use about the smallest possible amount of memory. On the down side, it turns out to be very slow for 3D algorithms.

The main equation we have to solve is

$$\begin{cases} u_t = Du \\ u_0 = g, \end{cases}$$

for some differential operator D . Again, this is solved explicitly at each time step since the size of the images does not allow to solve implicitly.

All 2D codes have been written within the ITK libraries, but for 3D algorithms, the ITK code was too slow (about 2min./iteration for an image of 50,000,000 voxels). Instead, we have written parallel C++ codes for solving unsteady equations, which are far more efficient. Running on 6 processors, runtime is now fairly small (about 3sec./iteration, depending on the complexity of the differential operator D). Below is a graph of the speed up as a function of the number of processors.

The computation time decreases dramatically by taking more processors. The images are split into layers that are distributed over the processors. At each time

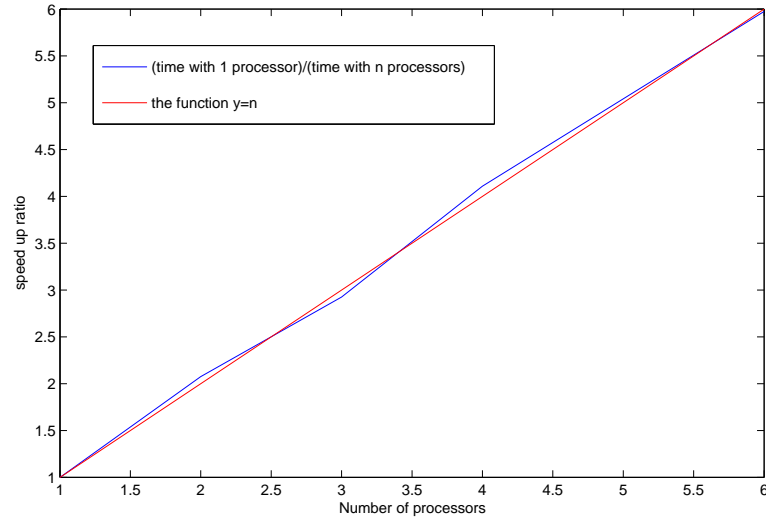


FIG. 4.15. The speed up of the algorithm. The speed up is calculated as follows: (time with one processor) divided by (time with n processors). The perfect speed up would be the function $y = n$. As we can see on the graph, the parallel gain is optimal in this case.

step, the processor computes the update of its layer and send the updated top and bottom slices to the corresponding processors. The communication is then very small. As the number of processors increase, there is more waiting time and the ratio of the number of slices that need to be exchanged and the total number of slices gets smaller. But this effect is not visible with 6 processors or less. The parallel gain is optimal.

The computing time at the second step of the segmentation process is obviously smaller. Also, the code becomes less and less parallelizable as we do more steps in the iterative segmentation process, since the domain to segment may become small, and can be contained in a region of the image that belongs to less processors. However, since the computing times are more than reasonable, we did not fix that issue.

INDEX

- Active contour model, 45
- Active Contour without edges, 54
- Active Contours, 45
- Anisotropic diffusion, 35

- Cacciopoli partition, 53

- Direct method, 26
- Distribution
 - Partial derivative, 16
 - Total derivative, 16

- Euler-Lagrange equation, 25

- Function
 - L^p , 11
 - Approximate discontinuity, 14
 - Approximate jump, 14
 - Approximate limit, 14
 - Bounded variation, 16
 - Bounded variation
 - Chain rule, 20
 - Coercive, 26
 - equiintegrable, 12
 - Lower-semi-continuous, 27
 - Piecewise constant function, 53
 - Signed distance, 59
 - Weak derivative, 16

- Heat equation, 33

- Image, 32
- Imaging
 - CT, 8
 - MRI, 5
 - Visible Human Project, 9

- Level Set method, 47

- Measure
 - Absolutely continuous, 14
 - Mutually singular, 14
 - Radon Measure
 - Compacity, 13
 - Definition, 12
 - Total variation, 12
 - Weak* convergence, 13
- Minimization Problem, 24
- Mumford-Shah functional, 50

- Poisson equation, 29

- Rudin, Osher, Fatemi model, 42

- Scheme
 - CrankNicholson, 33
 - Explicit scheme, 33
 - Implicit scheme, 33
 - Semi-explicit, 44
- Set
 - Approximate discontinuity set (S_u), 14
 - Finite perimeter, 17
 - Jump set (J_u), 14
 - Perimeter, 17
- Snake, 45
- Sobolev smoothing, 38
- Space

$\mathcal{D}(\Omega)$, 15

$\mathcal{M}(X)$, 13

$C_0(X)$, 13

$H^1(\Omega)$, 16

L^p , 11

Bounded variation

$BV(\Omega)$, 16

Cantor part, 19

Compactness, 18, 24

Jump part, 19

Sobolev part, 18

weak*-convergence, 18

Distributions ($\mathcal{D}'(\Omega)$), 15

Reflexive, 28

Sobolev $W^{1,p}(\Omega)$, 16

Theorem

Radon-Nikodým, 14

Riesz, 13

Weak derivatives, 16

BIBLIOGRAPHY

- [1] Luigi Ambrosio, Nicola Fusco, and Diego Pallara. *Functions of bounded variation and free discontinuity problems*. Oxford Mathematical Monographs. The Clarendon Press Oxford University Press, New York, 2000.
- [2] Gilles Aubert and Pierre Kornprobst. *Mathematical problems in image processing*, volume 147 of *Applied Mathematical Sciences*. Springer, New York, second edition, 2006. Partial differential equations and the calculus of variations, With a foreword by Olivier Faugeras.
- [3] Jean-François Aujol, Guy Gilboa, Tony Chan, and Stanley Osher. Structure-texture image decomposition—modeling, algorithms, and parameter selection. *Int. J. Comput. Vision*, 67(1):111–136, 2006.
- [4] Andrea Braides. *Approximation of free-discontinuity problems*, volume 1694 of *Lecture Notes in Mathematics*. Springer-Verlag, Berlin, 1998.
- [5] V. Caselles, R. Kimmel, and G. Sapiro. Geodesic Active Contours. *International Journal of Computer Vision*, 22(1):61–79, 1997.
- [6] T. F. Chan and L. A. Vese. Active contours without edges. *Image Processing, IEEE Transactions on*, 10(2):266–277, 2001.
- [7] Tony F. Chan, Selim Esedoglu, and Mila Nikolova. Algorithms for finding global minimizers of image segmentation and denoising models. *SIAM Journal on Applied Mathematics*, 66(5):1632–1648, 2006.
- [8] Tony F. Chan and Jianhong Shen. *Image processing and analysis*. Society for Industrial and Applied Mathematics (SIAM), Philadelphia, PA, 2005. Variational, PDE, wavelet, and stochastic methods.
- [9] Enrico Giusti. *Minimal surfaces and functions of bounded variation*, volume 80 of *Monographs in Mathematics*. Birkhäuser Verlag, Basel, 1984.
- [10] Enrico Giusti. *Direct methods in the calculus of variations*. World Scientific Publishing Co. Inc., River Edge, NJ, 2003.

- [11] X. Han, C. Xu, and J.L. Prince. A topology preserving level set method for geometric deformable models. *Pattern Analysis and Machine Intelligence, IEEE Transactions on*, 25(6):755–768, 2003.
- [12] M. Kass, A. Witkin, and D. Terzopoulos. Active contour models. *First International Conference on Computer Vision*, pages 259–268, 1987.
- [13] TY Kong and A. Rosenfeld. Digital topology: introduction and survey. *Computer Vision, Graphics, and Image Processing*, 48(3):357–393, 1989.
- [14] Triet M. Le and Luminita A. Vese. Image decomposition using total variation and $\text{div}(\text{bmo})$. *Multiscale Modeling & Simulation*, 4(2):390–423, 2005.
- [15] J. Lie, M. Lysaker, and X.C. Tai. A variant of the level set method and applications to image segmentation. *Math. Comp*, 75:1155–1174, 2006.
- [16] David Mumford and Jyant Shah. Optimal approximation by piecewise smooth functions and associated variational problems. *Communications on Pure Applied Mathematics*, 42:577–685, 1989.
- [17] Stanley Osher and James A. Sethian. Fronts propagating with curvature-dependent speed: algorithms based on Hamilton-Jacobi formulations. *J. Comput. Phys.*, 79(1):12–49, 1988.
- [18] P. Perona and J. Malik. Scale-space and edge detection using anisotropic diffusion. *IEEE Transactions on Pattern Analysis and Machine Intelligence*, 12(7):629–639, 1990.
- [19] Leonid I. Rudin, Stanley Osher, and Emad Fatemi. Nonlinear total variation based noise removal algorithms. *Phys. D*, 60(1-4):259–268, 1992.
- [20] Walter Rudin. *Principles of mathematical analysis*. McGraw-Hill Book Co., New York, third edition, 1976. International Series in Pure and Applied Mathematics.
- [21] Walter Rudin. *Functional analysis*. International Series in Pure and Applied Mathematics. McGraw-Hill Inc., New York, second edition, 1991.
- [22] J. A. Sethian. *Level set methods and fast marching methods*, volume 3 of *Cambridge Monographs on Applied and Computational Mathematics*. Cambridge University Press, Cambridge, second edition, 1999. Evolving interfaces in computational geometry, fluid mechanics, computer vision, and materials science.

- [23] Michael Struwe. *Variational methods*, volume 34 of *Ergebnisse der Mathematik und ihrer Grenzgebiete. 3. Folge. A Series of Modern Surveys in Mathematics [Results in Mathematics and Related Areas. 3rd Series. A Series of Modern Surveys in Mathematics]*. Springer-Verlag, Berlin, third edition, 2000. Applications to nonlinear partial differential equations and Hamiltonian systems.
- [24] Luminita A. Vese and Tony F. Chan. A multiphase level set framework for image segmentation using the mumford and shah model. *Int. J. Comput. Vision*, 50(3):271–293, 2002.
- [25] William P. Ziemer. *Weakly differentiable functions*, volume 120 of *Graduate Texts in Mathematics*. Springer-Verlag, New York, 1989. Sobolev spaces and functions of bounded variation.